Biostratigraphy, carbon isotope and sequence stratigraphy of South Tethyan Valanginian successions in the Essaouira-Agadir Basin (Morocco)

Stéphane Reboulet, Etienne Jaillard, Majd Shmeit, Fabienne Giraud, Moussa Masrour, Jorge Spangenberg

Biostratigraphy, carbon isotope and sequence stratigraphy of South Tethyan Valanginian successions in the Essaouira-Agadir Basin (Morocco)

Stéphane Reboulet[1], Etienne Jaillard[2], Majd Shmeit[2,3], Fabienne Giraud[2], Moussa Masrour[4], Jorge E. Spangenberg[5]

1. Univ. Lyon, Univ. Lyon 1, ENSL, CNRS, LGL-TPE, F-69622, Villeurbanne, France
2. Univ. Grenoble Alpes, Univ. Savoie Mont Blanc, CNRS, IRD, Univ. Gustave Eiffel, ISTerre, 38000 Grenoble, France
3. Lebanese University, Doctoral School of Science and Technology, Laboratory of Geosciences Georesources and Environment L2GE, EDST/PRASE, Beirut, Lebanon
4. Université Ibn Zohr, Faculté des Sciences, Département de Géologie, BP 8106, Cité Dakhla, Agadir, Morocco
5. University of Lausanne, Institute of Earth Surface Dynamics (IDYST), CH-1015 Lausanne, Switzerland

Corresponding author, S. Reboulet, e-*mail address:* stephane.reboulet@univ-lyon1.fr

Abstract

A detailed stratigraphic analysis was carried out on Valanginian deposits of six Moroccan sections of the Essaouira-Agadir Basin (EAB, South Tethyan margin) in order to characterize the Weissert Event and propose correlations with the North Tethyan margin (south–east France Basin). The studied successions consist of alternating marlstone and limestone beds with sandy intercalations, and are well exposed and relatively rich in ammonites. Ammonite biostratigraphy and sequence stratigraphy were established for all successions, whereas

calcareous nannofossil and carbon stable isotope analyses were performed for two and five sections, respectively. For each succession, an accurate ammonite zonal scheme allows to recognize the standard zonation established for the Mediterranean Province. A calcareous nannofossil zonation is provided for Zalidou and Aït Hamouch, considered as reference sections. The detailed biozonations allowed to ascribe an accurate age for most of the sedimentary discontinuities and depositional sequences identified in the EAB. East–west and north–south transects are established for the Valanginian depositional system. Despite some stratigraphic gaps, the Valanginian carbon isotope excursion (CIE) was recognized in most of the studied sections. The Moroccan successions are correlated with those of reference sections of south–east France i.e., the Vocontian Basin (Vergol-La Charce) and Provence Platform (Carajuan), using bio-sequence-chemo-stratigraphy. These inter-basin correlations allowed to evidence major "mid-Valanginian" and upper Valanginian eustatic regressions; the possible role of tectonics and glacio-eustacy is also discussed.

Keywords

Ammonite, Calcareous nannofossil, Depositional sequence, Weissert Event, Morocco, Inter-basin correlation

1. Introduction

Several significant palaeoceanographic, palaeoclimatic and palaeoenvironmental changes are recorded in Valanginian times (Gale et al., 2020). The South Atlantic Ocean began to open and the early stages of rifting were accompanied by extrusion of the Parana-Etendeka large igneous province (Coffin and Eldholm, 1994; Gomes and Vasconcelos, 2021). A cooling of the climate is recorded at least locally (Price, 1999; Pucéat et al., 2003). A biosphere crisis is suspected through a global carbon-cycle perturbation recorded by positive carbon isotope

excursion in marine carbonates and terrestrial organic matter, named the Valanginian Weissert oceanic anoxic event or the Weissert Event (Erba et al., 2004; Gröcke et al., 2005; Kujau et al., 2012). For these reasons, Valanginian successions have been extensively studied in the North Tethyan margin, where numerous detailed lithological, biostratigraphic, sedimentological and isotopic data are available (Lini et al., 1992; Föllmi et al., 1994; Hennig et al., 1999; Sprovieri et al., 2006; McArthur et al., 2007; Gréselle et al., 2011; Charbonnier et al., 2017; Aguado et al., 2018). As a result, reference sections are mainly located in south–east France, such as Vergol (Montbrun-les-Bains, Drôme), candidate section for the Valanginian Global Boundary Stratotype Section and Point (GSSP, Blanc et al., 1994; Kenjo et al., 2021) and La Charce (Drôme), GSSP for the Hauterivian (Mutterlose et al., 2020). Elsewhere, however, integrated studies are quite rare (e.g., Aguirre-Urreta et al., 2019), and works on the Valanginian period focused on ammonite biostratigraphy (e.g., Rawson, 2007), calcareous nannofossils zonation (e.g., Bralower, 1987; Bralower et al., 1989), synsedimentary tectonics (e.g., Masse and Lesbros, 1987; Gradinaru et al., 2016), sedimentary geochemistry and palaeoclimatology (e.g., Pucéat et al., 2003; Charbonnier et al., 2020).

In the South Tethyan margin of Africa, Lower Cretaceous deposits are commonly represented by clastic subaerial sediments ("Continental Intercalaire", Lefranc and Guiraud, 1990; Fanti et al., 2012; Newell et al., 2015), and marine sediments are restricted to the distal parts of the North-African margin. However, the latter are often deformed by the Alpine orogeny (Frizon de Lamotte et al., 2000) that makes difficult their study. Therefore, the Valanginian series are poorly known, and the Weissert Event is not documented by carbon isotope data, in spite of some integrated stratigraphy studies in northern Tunisia (Soua, 2016; Melliti et al., 2019; Ben Ammar and Layeb, 2021). The Moroccan Essaouira-Agadir Basin is located at the western edge of the High Atlas Mountain Range and on the Atlantic coast of Morocco. The basin belonged, therefore, to the southern margin of the Mesozoic Tethys Ocean. It offers a rare

opportunity to study the Valanginian stage, since it presents excellent outcrops ranging from outer shelf to nearshore environments (Ferry et al., 2007) and the Valanginian successions are rich in ammonites (Wippich, 2003; Ettachfini, 2004). Recently, the mid–Valanginian carbon isotope excursion has been identified for the first time in the deposits of the Essaouira-Agadir Basin (Shmeit et al., 2022). Six sections located in this basin provide ideal successions for an integrated approach owing to the well-exposed outcrops and relatively abundant ammonite records. The sections were also chosen to establish two transects: one in a south–north direction with Aït Hamouch, Zaouia Sidi Abderahmane and Zalidou; and one in a west–east direction with Obbay, Igouzoulen and Ida w Iddar. Except for the two latter sites, the successions were studied mainly for the ammonite content by Wippich (2001; 2003) and/or Ettachfini (2004).

The main goals of the study were: (1) to establish a well-constrained integrated stratigraphic framework of the upper Berriasian–lowermost Hauterivian interval of the Essaouira-Agadir Basin, based on a high-resolution biostratigraphy involving ammonite and calcareous nannofossil biozonations, and carbon isotope stratigraphy, thus allowing a characterization of the Weissert Event in the South Tethyan margin; (2) to define time lines, based on the analysis of the evolution of sedimentary depositional environments, discontinuity surfaces and sequence analysis; and (3) to correlate the studied sections of the Essaouira-Agadir Basin with those of south–east France Basin in order to discriminate local from global factors, that influence sedimentary palaeoenvironments.

To shorten the manuscript, some abbreviations are used. Essaouira-Agadir Basin, EAB. South–east, SE. Formation, Fm. Sequence boundary, SB. “Discontinuité du Valanginien moyen”, DVM. “Discontinuité du Valanginien supérieur”, DVS. “Discontinuité du Valanginien terminal”, DVT. “Discontinuité au toit des Calcaires Blancs”, DCB. Hummocky cross stratification, HCS. First occurrence, FO. Last occurrence, LO. First appearance datum,

FAD. Last appearance datum, LAD. For the ammonite zonation: Standard zone, StZ; Standard subzone, StSz; Local subzone, LSz. Carbon isotope excursion, CIE. Deep Sea Drilling Project, DSDP. For the stratigraphic position of fossils, an alphanumeric notation is used with the abbreviation of the name of the section followed by the bed number: Aït Hamouch, AH or AtH; Zalidou, ZA; Zaouia Sidi Abderahmane, ZS; Igouzoulen, IGb or IGz; Ida w Iddar, IW; Obbay, OB.

2. Geological setting

The EAB belongs to the Western Atlas Chain. It is part of the Atlantic passive margin, the evolution of which can be divided into a rifting phase (Late Permian–Late Triassic), a drifting phase (Early Jurassic–Turonian) and an Atlasian deformation period. The first compressional deformation was of Santonian–Campanian age, followed by the Eocene–Pleistocene Alpine deformation which gently folded the EAB (Guiraud and Bosworth, 1997; Algouti et al., 1999; Frizon de Lamotte et al., 2000; 2009; Zühlke et al., 2004; Hafid et al., 2008). During the Early Cretaceous, the EAB was dominated by an extensional regime (Le Roy et al., 1998) and a low thermal subsidence rate (Ellouz et al., 2003; Bouatmani et al., 2007). After drowning of the Upper Jurassic–Berriasian carbonate shelf, deposition in the EAB is first dominated by marl accumulation with scarce limestone beds (Valanginian–Hauterivian), then by a marlstone-limestone succession (Barremian–Aptian) with a coarse sandy intercalation (upper Barremian) and finally, by a thick shaly series (Albian) capped by upper Albian limestones (Ambroggi, 1963; Wiedmann et al., 1982; Canérot et al., 1986; Rey et al., 1988; Witam, 1998; Bourgeoini et al., 2002; Ferry et al., 2007; Luber et al., 2017; Jaillard et al., 2019a; 2019b; Gale, 2020).

In the EAB, west-sloping Mesozoic strata rest on the Hercynian rocks of the High Atlas (Fig. 1). The EAB comprises two main, east–west trending folds, which divide it in three parts. The southern part constitutes the southern flank of the Imouzzer anticline, the core of which offers

large outcrops of Jurassic rocks. The central part is comprised between the Imouzzer and the Amsittene anticlines, and includes a mild anticline located south of Tamanar (Fig. 1). The northern part is located north of the Amsittene anticline and has not been studied here.

The first comprehensive works to understand the stratigraphy of the EAB were by Roch (1930) and Ambroggi (1963) who provided major contributions, and Duffaud et al. (1966). An overview of the Cretaceous sedimentary succession of the EAB has been given by Wiedmann et al. (1982). According to Duffaud et al. (1966), Rey et al. (1986; 1988) and Taj-Eddine et al. (1992), the uppermost Tithonian–lowermost Hauterivian interval comprises four formations (Fig. 2). The Cap Tafelney Fm is made of bryozoan-rich limestones overlain by calpionellid-rich limestone beds, which allowed to ascribe the unit to the uppermost Tithonian–Berriasian. The fossiliferous Aghroud Oudar Fm (lower Valanginian), comprises alternating marlstone and argillaceous limestone beds. The Sidi Lhoussaine Fm, ascribed to the upper Valanginian and lower Hauterivian, consists of green marlstone, with few limestone beds at the base and sand beds at the top. The Tamanar Fm (lower Hauterivian), is defined as a reefal limestone unit. The limits of these units, however, are not well defined.

Detailed palaeontological studies based on ammonites of the uppermost Berriasian–lowermost Hauterivian interval have been performed by Ettachfini (1991; 2004) and Wippich (2001; 2003). Their rigourous works on the systematics of Valanginian fauna allowed to show taxonomic misinterpretations of some Valanginian neocomitids and olcostephanids, and to propose new bio-chronostratigraphic results. For example, Wippich (2003) recognized most of the ammonite (sub-)zones of the standard zonation of the Mediterranean Province proposed by Hoedemaeker et al. (2003). Wippich (2003) identified, for the first time, ammonite markers to characterize the Valanginian–Hauterivian boundary that is placed within a thick marly series corresponding to the Sidi Lhoussaine Fm of Rey et al. (1986; 1988).

From a sedimentological point of view, Rey et al. (1986; 1988) identified two major sedimentary discontinuities, at the top of the Berriasian Cap Tafelney Fm, and at the base of the lower Hauterivian Tamanar Fm, respectively. Minor discontinuities are also mentioned in the upper part, and at the top, of the Aghroud Oudar Fm (lower Valanginian), and within the Sidi Lhoussaine Fm (upper Valanginian–lower Hauterivian). These authors also determined a transgressive trend at the base of the Valanginian, and a transgressive trend through Valanginian times, locally interrupted by an emergence period near the lower–upper Valanginian boundary. Ferry et al. (2007) provided detailed, well-dated sections of the Berriasian–Hauterivian series (Fig. 2). They interpreted the Valanginian series as deposits of a shallow mixed, carbonate-clastic shelf. According to these authors, the Berriasian and lower Valanginian deposits are an overall east-ward retrograding system. The base of the upper Valanginian shows a significant transgressive trend, and the lowermost Hauterivian is marked by a sudden subsidence pulse which causes a new transgression, followed by a major progradation in the upper part of the lower Hauterivian (Fig. 2; Ferry et al., 2007).

3. Materials and methods

Among the six studied sections, one is located in the southern part of the basin, while the other sections belong to its central part; their GPS coordinates are given in Appendix A, (Tab. A1, Supplementary material). Altogether, they define a north–south and an east–west profile (Fig. 1). These sections correspond to the external part of the EAB. For an east–west profile of the southern part of the EAB, see Ferry et al. (2007). The Zalidou section is located north–east of the village Ida w Tghouma and was already described by Ettachfini (2004). The Aït Hamouch and Zaouia Sidi Abderahmane sections are located on the southern and northern side of the Imouzzer anticline, respectively. The former was described by Wippich (2001; 2003), Ettachfini (2004) and Ferry et al. (2007), and the latter corresponds to the Zaouia Sidi

Abd-er-Rahmane and Taourirt Oubazine sections of Wippich (2001; 2003) and to the Zawiat Si Abd A-Rahmane of Ettachfini (2004). The Igouzoulen section has been studied along the Igouzoulen river, a few km west of the Tamanar-Smimou road. The Ida w Iddar and Obbay sections belong to the southern flank of the Amsittene anticline. The latter was already studied by Ettachfini (2004).

The fossils and rock samples were collected in Morocco and exported in France within the framework of the project "MA/13/291-PHC-Volubilis" and according to the national legislation of Moroccan authorities; documents and sampling-export certifications are given in Appendix B (Supplementary material).

3.1. Sedimentology. The sections were studied and measured bed by bed. Most sedimentological observations (lithology, texture, sedimentary features, macrofossil content, bioturbation, minerals) were made on the field. Samples were collected in limestone beds, and thin sections were prepared for microfacies analysis. Because the Valanginian–lowermost Hauterivian succession is mainly made of marlstone, facies were chiefly defined through field observations, locally completed by few microfacies analysis of limestone beds.

3.2. Ammonites. 1344 specimens of ammonites were recolted in the six studied sections; no aptychus has been observed. The sampling was mainly done from Valanginian limestone beds. The uppermost part of the Berriasian and the basal part of the Hauterivian were also sampled in some sections. Only specimens well-preserved enough to allow an identification were transferred to the laboratory (Lyon, France), where extraction was completed using a vibratory device, and determination was effectuated using a palaeontological worksheet. Specimens doubtfully identified are indicated by a question mark. Dissolution of shells is usual and ammonites are generally preserved as internal calcareous moulds. Lower

Valanginian ammonites are relatively well preserved and may reach a large size. Upper Valanginian specimens are more often fragmented and crushed. A few dozens of pyritized specimens were found in marlstone of the upper Valanginian. The specimens are recorded as "Collection Reboulet" with the label "UJF-ID" that means "Université Joseph Fourrier – Institut Dolomieu" belonging to the OSUG Collections; OSUG-COLLECTIONS is a database of rocks, minerals and fossils (https://web.collections.osug.fr, OSUG, UGA. doi:10.5072/OSUG-COLLECTIONS.all).

3.3. Calcareous nannofossils. A total of 90 and 55 samples, selected from calcareous clay to limestone, and collected in the Zalidou and Aït Hamouch sections, respectively, were investigated for calcareous nannofossil biostratigraphy (Shmeit et al., 2022; this work). These two sections are more extended and are characterized by more marly intervals with respect to the other sections; and were, therefore, more suitable for nannofossil sampling. Studied samples from the composite Aït Hamouch section corresponded to the "AH" section, except for the interval between 32 and 42 m, where the studied samples were collected from the "AtH" section. Methods of smear slide preparation, counting and evaluation of the nannofossil preservation, as well as taxonomic framework and zonations used here were described in Shmeit et al. (2022). The smear slides are numbered as "UJF-ID" (Université Joseph Fourrier – Institut Dolomieu) and curated in the OSUG Collections (for the database, the URL is indicated in part 3.2).

3.4. Carbon stable isotopes. The analysis was performed on 291 whole rock samples from the studied sections, except Obbay, at the stable isotope laboratories of the Institute of Earth Surface Dynamics of the University of Lausanne. Analyses where done using a Thermo Fisher Scientific Gas Bench II carbonate preparation device connected to a Delta Plus XL

isotope ratio mass spectrometer. The CO_2 extraction was done at 70°C. The carbon isotope ratios were reported in the delta (δ) notation as the per mil (‰) relative to the Vienna Pee Dee belemnite standard (VPDB), where δ = (Rsample – Rstandard)/Rstandard and R = $^{13}C/^{12}C$. The measured $\delta^{13}C_{carb}$ values were normalized to the VPDB scale by calibration of the reference gases and working standards with international reference materials NBS 18 (carbonatite, $\delta^{13}C$ = -5.01 ‰) and NBS 19 (limestone, $\delta^{13}C$ = +1.95 ‰). Analytical uncertainty (1 sigma), monitored by replicate analyses of the international calcite standard NBS 19 and the laboratory standard Carrara Marble ($\delta^{13}C$ = +2.05 ‰) was not greater than +/-0.05‰ for $\delta^{13}C$.

4. Results and interpretations

4.1 Ammonite stratigraphy: zonation and chronostratigraphic subdivisions

The ammonite fauna of the six studied Moroccan sections (Figs. 3–8) consists of 33 genera grouped into 7 families, using the supra-classification proposed by Klein (2005) and Klein et al. (2007; 2009), partly modified. The classification used here and the authorship of generic and specific names are shown in the taxonomic list provided in Appendix C (Supplementary material). The systematic revision of species was mainly based on the monographies of Le Hégarat (1973), Company (1987), Bulot (1995), Reboulet (1996), Joly (2000), Wippich (2001), Ettachfini (2004), Busnardo (*in* Gauthier et al., 2006) and Kenjo (2014). Further information on stratigraphy and taxonomy is available in the papers by Thieuloy (1977), Busnardo and Thieuloy (1979), Thieuloy et al. (1990), Reboulet et al. (1992), Thieuloy and Bulot (1992), Bulot et al. (1993), Bulot and Thieuloy (1995), Aguirre-Urreta and Alvarez (1999), Reboulet and Atrops (1999), Busnardo et al. (2003), Wippich (2003), Reboulet (2008), Company and Tavera (2015), Mourgues et al. (2015), Aguado et al. (2018) and

Vašíček (2020). Palaeontological comments and illustrations are given for some taxa in Appendix D (text and Figs. D1–D7, Supplementary material).

The analysis of the ammonite stratigraphic distribution allowed to establish a zonal scheme for the studied sections. The standard ammonite zonation built by the International Union of Geological Sciences Kilian Group (Hoedemaeker et al., 2003; Reboulet et al., 2006; 2009; 2011; 2014; 2018) for the Mediterranean Province of the Mediterranean–Caucasian Subrealm (Tethyan Realm) is applied here. Only two regional units are added, namely the *N. subtenuis* and *B. campylotoxus* local subzones, in order to make easier the comparisons with previous works of Wippich (2001; 2003) and Ettachfini (2004). The ammonite zones are interval zones and are defined by the interval between the FAD of two successive ammonite-indices (Hedberg, 1976). In order to correlate more precisely biostratigraphic subdivisions with ammonite evolution, the boundaries of the Valanginian interval zones correspond to major changes in the ammonite fauna (Reboulet and Atrops, 1999, Kenjo, 2014; Company and Tavera, 2015; Kenjo et al., 2021); this allows a better faunal characterization of the zones. The chronostratigraphic subdivisions (Berriasian–Valanginan, lower–upper Valanginian and Valanginian–Hauterivian boundaries) are characterized in terms of ammonite markers.

The *Tirnovella alpillensis* Standard Zone – uppermost Berriasian. According to the Kilian Group (Reboulet et al., 2018), the *T. alpillensis* StZ is the last zone of the Berriasian (for detailed information see Kenjo et al., 2021). The index-species was found in the Zalidou, Zaouia Sidi Abderahmane and Obbay sections (Figs. 3, 5, 8). However, as the sampling was low in the lower part of the successions, the FO of *T. alpillensis* cannot be used here to place the base of the zone. Also, the *T. alpillensis* StZ is more or less well-recognized in the studied sections by the occurrence of some quite characteristic taxa of the upper Berriasian like *Fauriella boissieri*, *Berriasella calisto*, *Malbosiceras rouvillei*, *Pomeliceras breveti*,

Spiticeras bulliforme, *Spiticeras ducale*, *Kilianiceras gratianopolitense*, *Negreliceras* sp., *Groebericeras* sp., *Ptychophylloceras (Semisulcatoceras) semisulcatum, Holcophylloceras silesiacum* and *Lytoceras honnoratianum.*

The "*Thurmanniceras*" *pertransiens* Standard Zone and the *Neocomites premolicus* Standard Subzone – Base of the Valanginian stage. Few specimens of "*T.*" *pertransiens* were found in the Zalidou, Aït Hamouch, Igouzoulen and Obbay sections (Figs. 3–4, 6, 8). In the latter site, the FO of this index-species is used to identify the base of the "*T.*" *pertransiens* StZ and thus the lower boundary of the Valanginian (OB13). Kenjo et al. (2021) discussed the choice of the primary marker to define the base of this stage, and gave the priority to the FAD of "*T.*" *pertransiens* rather than the FAD of *Calpionellites darderi*. As the index-species of "*T.*" *pertransiens* is rare or even absent in most of the Moroccan sections, the base of the zone can be placed with the FO of *N. premolicus* (Ettachfini, 2004; this work, ZA20, AH60, ZS34, IGz18; IW5; Figs. 3–7). Taking in account the systematic and biostratigraphic characteristics of *N. premolicus* shown by Ettachfini (2004), Kenjo (2014) and Company and Tavera (2015), the Kilian Group agreed to introduce the *N. premolicus* Subzone in the standard zonation (Reboulet et al., 2018). This subzone starts at the base of the "*T.*" *pertransiens* StZ and ends at the LO of *N. premolicus*. Because the upper part of the zone is not characterised by a subzone for the moment, the *N. premolicus* StSz is provisionaly considered as a total range subzone. For Wippich (2003), the simultaneous FO of *N. premolicus* and the genus *Sarasinella* is a workable alternative to put the base of the "*T.*" *pertransiens* StZ. Except for *Sarasinella trezanensis* that would appear in the uppermost part of the Berriasian, Ettachfini (2004; tab. 5, p. 82) also noted the co-occurrence of "*T.*" *pertransiens*, *N. premolicus*, *Sarasinella eucyrta* and *Sarasinella longi* at the base of the Valanginian. The simultaneous FO of *N. premolicus* with *S. longi* or *S. eucyrta* are recorded at the base of the "*T.*" *pertransiens* StZ in the Zalidou and Aït Hamouch sections, respectively (Figs. 3–4). These two species of *Sarasinella* and *S.*

trezanensis are also recorded in the rest (mainly in the lower part) of the "*T.*" *pertransiens* StZ in most of the studied sections (Figs 3–5, 7–8). In most of the Moroccan studied sections (Figs. 3–6, 8), *"Thurmanniceras" gratianopolitense* takes place in the "*T.*" *pertransiens* StZ; in Aït Hamouch, Igouzoulen and Obbay sites, this species first occurs at the base of the zone. Considering that the specimens of *"Thurmanniceras" thurmanni* studied by Wippich (2001; 2003) may be (partly?) interpreted as "*T.*" *gratianopolitense* (see Kenjo et al., 2021), it seems that this species could appear in the *T. alpillensis* StZ as shown in figures of synthetic ranges of taxa provided by Wippich (2001, tab. 15; 2003, fig. 10). According to his sections showing ammonite ranges, "*T.*" *thurmanni* occurs in the "*T.*" *pertransiens* StZ, except in Addar, where the appearance of "*T.*" *thurmanni* occurs in bed 105 dated from the uppermost part of the Berriasian by this author. The specimen illustrated in Wippich (2001, "*T.*" *thurmanni*, pl. 20, fig. 1) and sampled in layer 105 is here interpreted as "*T.*" *gratianopolitense*. The layer 105 of Wippich (2001) could be dated from the "*T.*" *pertransiens* StZ as the last typical Berriasian taxa occur in layer 104 and the first typical Valanginian taxa appear just above in layer 106. Moreover, it seems that Wippich (2001; 2003) identified the base of the "*T.*" *pertransiens* StZ in the Aït Hamouch section with the FO of his "*T.*" *thurmanni*. Ettachfini (2004; tab. 5) also indicated the occurrence of "*T.*" *gratianopiltense* in the uppermost part of the Berriasian. In his sections showing the ammonite distributions (Addar, Sidi Yahia Ou Saïd, Zalidou, and Akoui Griz), specimens of this species were found in the top part of the *T. alpillensis* Subzone; however, at least for some of these sections, this interval could be alternatively dated as lowermost Valanginian. The difference in the ranges of "*T.*" *gratianopolitense* (Wippich (2001; 2003) and Ettachfini (2004) *versus* Company and Tavera (2015) and this work), may be also explained by a different conception of this species. Four specimens of *Thurmanniceras*? were found in the *T. alpillensis* StZ of the Ida w Iddar section (Fig. 7, IW2b); they may correspond to true "*T.*" *thurmanni*, as this species is recorded in the

uppermost part of the Berriasian by Ettachfini (2004). These comments on the stratigraphic distribution of *Thurmanniceras* around the Berriasian–Valanginian boundary interval show that a revision of this genus is needed. Regarding *Kilianella*, this genus is only observed in the upper part of "*T.*" *pertransiens* StZ in the Aït Hamouch (Fig. 4) and Ida w Iddar sections (Fig. 7; one specimen of *Kilianella lucencis*?). This is in accordance with other data on the Moroccan western High Atlas given by Ettachfini (2004; occurrence of *Kilianella* sp. 1 in the upper part of his *N. premolicus* Zone); Wippich (2001; 2003) did not record *Kilianella* in the "*T.*" *pertransiens* StZ. In summary, the (co-) occurrences of "*T.*" *pertransiens*, "*T.*" *gratianopolitense*, *N. premolicus*, *S. longi* and/or *S. eucyrta* allow to place the base of the Valanginian and provide a good characterisation of the "*T.*" *pertransiens* StZ of all the studied sections (Figs. 3–8).

The *Neocomites neocomiensiformis* Standard Zone; *Neocomites subtenuis* and *Busnardoites campylotoxus* local subzones. The *N. neocomiensiformis* StZ is applied for the first time in the Moroccan lower Valanginian successions. It could not be integrated in the zonal schemes of Wippich (2003) and Ettachfini (2004) as this zone was proposed by Company and Tavera (2015). This index-species is relatively rare and only found in the upper part of the zone in the Zalidou, Aït Hamouch, Igouzoulen, Ida w Iddar and Obbay sections. Consequently, the base of the zone is identified in the six studied Moroccan sections by the FO of *N. subtenuis* (Figs. 3–8, ZA25, AH72, ZS43b, IGz23, IW15b and OB18) as its appearance is contemporaneous with that of *N. neocomiensiformis* in SE Spain (Company and Tavera, 2015). In terms of stratigraphic interval, the *N. subtenuis* LSz (Ettachfini, 2004) used here corresponds to the *Baronnites hirsutus* Subzone proposed by Company and Tavera (2015). Indeed, the FO of *N. subtenuis* is simultaneous to that of *B. hirsutus* (Company and Tavera, 2015) and the upper boundary of these subzones is defined by the FAD of *B. campylotoxus* (Ettachfini, 2004) and *Valanginites dolioliformis* (Company and Tavera, 2015),

respectively; according to the latter authors, the appearance of these both species is contemporaneous. It is difficult to characterize the *N. subtenuis* LSz in the Moroccan sections because the assemblage is poor and *B. hirsutus* was not identified (Wippich, 2001; 2003; Ettachfini, 2004; this work). In the *N. subtenuis* LSz, rare *Sarasinella uhligi* and/or *Karakaschiceras paraplesium* have been recorded in the Zalidou, Aït Hamouch and Igouzoulen sections (Figs. 3–4, 6). The occurrence of *S. uhligi* in the zonal scheme of Wippich (2003, fig. 10) allows to identify the *N. subtenuis* LSz in the upper part of his "*T.*" *pertransiens* StZ. In the same interval, specimens identified by Wippich (2001; 2003) as *N. neocomiensis* may be partly interpreted as *N. subtenuis*. The range of *K. paraplesium* is concordant with that observed in SE Spain (mainly in the *B. hirsutus* Subzone of Company and Tavera, 2015, fig. 7). In the Aït Hamouch and Ida w Iddar sections (Figs. 4, 7), *Kilianella roubaudiana* is recorded in the *N. subtenuis* LSz. Some specimens identified with doubt to *Luppovella* were observed in the lower part of the *N. subtenuis* LSz in the Aït Hamouch section (Fig. 4). This agrees with the data of Ettachfini (2004) as this author observed the appearance of this genus at the base of this subzone. However, contrary to the observation made in SE Spain by Company and Tavera (2015, fig. 7), *Luppovella superba* has never been recorded in the upper part of the "*T.*" *pertransiens* StZ of the Moroccan series (Wippich, 2001; 2003; Ettachfini, 2004; this work). This is in agreement with Kenjo (2014) and Kenjo et al. (2021), who noted in SE France the FO of *L. superba* in the *N. neocomiensiformis* StZ (see also Bulot (1995), who indicated this event in his *Olcostephanus stephanophorus* Zone). In the upper part of the *N. neocomiensiformis* StZ, the base of the *B. campylotoxus* LSz is placed at the FO of its relatively abundant index-species (Figs. 3–8, ZA29, AH78, ZS47, IGz26a, IW19 and OB21). Also, this subzone is well characterized by *L. superba* and numerous *Olcostephanus guebhardi* (first acme of this olcostephanid; Zalidou, Aït Hamouch, Zaouia Sidi Abderahmane, Igouzoulen and Ida w Iddar, Figs. 3–7). This assemblage is observed by

Wippich (2001; 2003) and Ettachfini (2004). In agreement with these authors, the last occurrences of *Luppovella* and/or *Kilianella* are recorded in this subzone, as well illustrated in the Aït Hamouch, Igouzoulen and Ida w Iddar sections (Figs. 4, 6–7). *Busnardoites subcampylotoxus*?, *Neohoploceras depereti* and *Lytoceras juilleti* were recorded (only one specimen for each species) in the Zalidou and Aït Hamouch sections (Figs. 3–4). The *B. campylotoxus* LSz corresponds, in terms of stratigraphic interval, to the *V. dolioliformis* Subzone of Company and Tavera (2015). Indeed, according to these authors, the FOs of both index-species are simultaneous and the upper limit of these subzones is defined by the FO of *Karakaschiceras inostranzewi* (see also Ettachfini, 2004; this work). However, *V. dolioliformis* is only recorded in the *B. campylotoxus* LSz of the Aït Hamouch and Igouzoulen sections (Figs. 4, 6).

The *Karakaschiceras inostranzewi* Standard Zone. The base of this zone is placed at the FO of its index-species (Figs. 3–8, ZA34a, AH87, ZS50, IGz27a, IW26 and OB22). The *K. inostranzewi* StZ corresponds to the *Karakaschiceras biassalense* Zone of Wippich (2001; 2003) and Ettachfini (2004). According to these authors, the fauna of this stratigraphic interval is little diversified. Among neocomitids, the FO of *Neocomites neocomiensis*, *Neocomites teschenensis* and *Neocomites platycostatus* are recorded in this zone at Zalidou and Obbay (Figs. 3, 8). Few *Neohoploceras* (FO of *Neohoploceras provinciale*; Aït Hamouch, Ida w Iddar and Obbay sections, Figs. 4, 7–8) are also represented. Bulot and Thieuloy (1995), Company and Tavera (2015) and Aguado et al. (2018) also recorded the FO of *N. provinciale* in the basal part of the *K. inostranzewi* StZ. Specimens of *O. guebhardi* (beginning of the second acme) were found in most sections (Figs. 3–5, 8).

The *Saynoceras verrucosum* Standard Zone; the *S. verrucosum* and *Karakaschiceras pronecostatum* Standard subzones – Base of the upper Valanginian substage. Wippich (2003) and Ettachfini (2004) emphasized the difficulty to identify the base of the *S.*

399 *verrucosum* StZ due to the scarcity of the index-species in the Moroccan successions. For
400 example, only a single specimen was found by Wippich (2001; 2003; Tarourirt Oubazine
401 section). Moreover, as noted by this author, the succession is highly condensed and the
402 thickness is much reduced around the lower (*K. inostranzewi* StZ)–upper (*S. verrucosum* StZ)
403 Valanginian boundary (see also this work). As the identification of this boundary is
404 problematic in the western High Atlas, Ettachfini (2004) chosed to place the base of the upper
405 Valanginian at the base of his *K. biassalense* Zone, as suggested by Bulot and Thieuloy
406 (1995) at the base of their *K. inostranzewi* Zone in SE France. Even though no specimen of *S.*
407 *verrucosum* was found in the six studied Moroccan sections (Figs. 3–8), this suggestion was
408 not followed here to agree with the standard zonation and its chronostratigraphic subdivisions
409 (Reboulet et al., 2018). In absence of *S. verrucosum*, the (base of the?) *S. verrucosum* StZ is
410 identified by the (first) occurrence of *Valanginites ventrotuberculatus* as recorded in the
411 Zaouia Sidi Abderahmane (ZS52), the Igouzoulen (IGz27c), and Obbay (OB24) sections
412 (Figs. 5–6, 8). Indeed, according to Company and Tavera (2015), the FOs of both these
413 species are simultaneous in SE Spain; their range ends in the basal part of the *S. verrucosum*
414 StZ and they do not co-occur with *K. pronecostatum* (Aguado et al., 2018), index-species of
415 the second subzone of the *S. verrucosum* StZ. In the Zaouia Sidi Abderahmane and Obbay
416 sections, *V. ventrotuberculatus* is found with *K. pronecostatum*. In the latter section,
417 *Saynoceras contestatum* is also recorded together with *K. pronecostatum* (OB24), as shown in
418 Ettachfini (2004, see tab. 5, p. 82). However their ranges do not overlap in SE France (Bulot
419 and Thieuloy, 1995) and SE Spain (Aguado et al., 2018). As *K. pronecostatum* appears in the
420 upper part of the zone, its co-occurrence with *S. contestatum* and *V. ventrotuberculatus* in
421 some Moroccan sections may be explained by a condensed lithology in the basal part of the
422 upper Valanginian (see above; this work), even though a mistake in the identication of these
423 specimens of *Karakaschiceras* cannot be excluded. For Ettachfini (2004), the base of the *S.*

verrucosum StZ is characterized by the FO of *O. guebhardi* morphe *querolensis* that is well represented in the lower part of his *S. verrucosum* horizon. This may correspond, at least partly, to the second acme of *O. guebhardi*, as observed at Zalidou, Igouzoulen, and Ida w Iddar (Figs. 3, 6–7). In Zalidou and Ida w Iddar sections, the base or the lower part of the *S. verrucosum* StZ is not well identified due to the absence of ammonite markers (*V. ventrotuberculatus* and *S. contestatum*). Thus, the second acme of *O. guebhardi* might be used to approximate the lower–upper Valanginian boundary; in this case, it could be put at the base of layers ZA36 (Fig. 3; boundary indicated by a dashed line) and IW29 (Fig. 7). This solution is applied for the latter section, in which typical ammonite markers of the lower part of the upper Valanginian are absent. In the Zalidou section, however, the FO of *K. pronecostatum* (ZA40, boundary indicated by a solid line) is used to place the base of the zone. According to Wippich (2003), *N. platycostatus* is restricted to the *S. verrucosum* StZ, as observed in the Zaouia Sidi Abderahmane and Igouzoulen sections (Figs. 5–6). However, this neocomitid is already present in the upper part of the *K. inostranzewi* StZ in the Obbay section (Fig. 8); similar observations were made in SE France (Reboulet, 1996; Reboulet and Atrops, 1999; in their *N. platycostatus* Horizon) and SE Spain (Company and Tavera, 2015; in their *S. contestatum* Subzone). Ettachfini (2004), who considered that *N. platycostatus* is a junior synonym of *N. teschenensis*, indicated the FO of this species at the base of the *K. inostranzewi* StZ. If the (base of the) *S. verrucosum* StZ cannot be identified by the FO of *N. platycostatus*, the latter species seems (more) abundant in this zone, as observed in the Zaouia Sidi Abderahmane and Obbay sections (Figs. 5, 8). It can be expected that the distribution of *N. platycostatus* recorded by Wippich (2003) only corresponds to the highest frequency of this species in the *S. verrucosum* StZ. As *Neocomites* gr. *platycostatus–teschenensis* are relatively well represented in layers ZA36–37 (Fig. 3), this interval of the Zalidou section could be dated to this zone, as previously evoked based on the abundance of *O. guebhardi* (cf. 2nd

449 acme). However, the lower boundary of this zone cannot be placed using the abundance
450 variations of some taxa that are partly controlled by palaeoenvironmental conditions (see
451 Reboulet et al., 2003) and sedimentary factors (cf. condensed layers). At Zaouia Sidi
452 Abderahmane (Fig. 5), one specimen of *Rodighieroites belimelensis* is recorded in the *S.*
453 *verrucosum* StZ; this is in agreement with Wippich's data (2003; in *K. pronecostatum* StSz).
454 In the Igouzoulen section (Fig. 6), *Neohoploceras submartini* occurs in the *S. verrucosum*
455 StZ; Ettachfini (2004) also observed this distribution. Taking into account that the LO of *N.*
456 *submartini* is recorded in the basal part of the *K. pronecostatum* StSz in SE Spain (Aguado et
457 al., 2018), the base of this subzone in the Igouzoulen section could be placed around the layer
458 IGz29b. However, this should be interpreted carefully as the ranges of *Neohoploceras* taxa
459 show some discrepancies (see Bulot and Thieuloy, 1995; Reboulet, 1996; Wippich, 2001;
460 2003; Ettachfini, 2004; Aguado et al., 2018); the same remark can be done for the distribution
461 of *Rodighieroites* taxa. In two Moroccan sections, *N. provinciale* occurs in the lower part of
462 the upper Valanginian. At Zaouia Sidi Abderahmane, this species co-occurs with *K.*
463 *pronecostatum* in the basal part of the *S. verrucosum* StZ (Fig. 5, ZS52–53). According to
464 Bulot and Thieuloy (1995) and Ettachfini (2004), *K. pronecostatum* seems to appear just after
465 the disappearance of *N. provinciale*. Thus, as evoked previously, this Moroccan ammonite
466 assemblage may be interpreted as a result of a condensed lithology and/or a misidentification
467 of some specimens because of the poor preservation of upper Valanginian ammonites. A
468 similar interpretation is made for the Aït Hamouch section, where *N. provinciale* and *K.*
469 *pronecostatum* also co-occur in layer AH89, with the record of *Neocomites peregrinus* and *K.*
470 *inostranzewi*? (Fig. 4). According to Ettachfini (2004) and Aguado et al. (2018), *K.*
471 *pronecostatum* and *N. peregrinus* do not co-occur but the ranges given by Bulot and Thieuloy
472 (1995) and Reboulet and Atrops (1999) show a short overlap of both species. Even though
473 there are some discrepancies in the distributions of *Neohoploceras* taxa (see references

above), it seems that *N. provinciale* never occurs with *N. peregrinus.* The layer AH89 is also characterized by the occurrence of few dubious specimens of *K. inostranzewi*?; their preservation might indicate that they have been reworked (cf. discontinuity D5; Fig. 4). To summarize, in most of the studied Moroccan sections, it is difficult to recognized clearly the lower subzone of the *S. verrucosum* StZ (and so its base) due to: a) the absence of the index-species and the rarity of some second ammonite markers as *V. ventrotuberculatus*; b) the condensed lithology and the possibility of reworking material related to the discontinuity D5.

The *Neocomites peregrinus* Standard Zone; the *N. peregrinus* and *Olcostephanus nicklesi* Standard subzones. In the western High Atlas, this zone was identified by Wippich (2001; 2003) and Ettachfini (2004). The index-species is recorded in three sections and its FO allows to place the base of the *N. peregrinus* (Sub-)Zone in the Zalidou (ZA41), Aït Hamouch (AH89), and Zaouia Sidi Abderahmane (ZS57) sections (Figs. 3–5). However, it is relatively difficult to characterize this interval as the ammonite assemblage is poor. When the index-species is absent, the boundary between the *S. verrucosum* and *N. peregrinus* zones can be approximated using the occurrence of *Olcostephanus balestrai* and/or *Oosterella gaudryi* (or *Oosterella* sp. ind.), as made at Igouzoulen (IGz33), Ida w Iddar (IW33) and Obbay (OB25) (Figs. 6–8). The *O. nicklesi* StSz is identified in the Obbay section by the FO of the index-species (OB28). Moreover, pyritized specimens of *Himantoceras acuticostatum* were also sampled in the same layer. The occurrence of *Himantoceras* sp. ind. in the Zalidou section (ZA46, Fig. 3) allows to recognize the *O. nicklesi* StSz. Indeed, these heteromorphs are known in the basal part of this subzone (Bulot and Thieuloy, 1995; Reboulet, 1996; Reboulet and Atrops, 1999; Ettachfini, 2004). According to Wippich (2003), the only record of the *O. nicklesi* StSz corresponds to reworked specimens of *O. nicklesi* and *Himantoceras trinodosum* found in a lag deposit at the base of the *Criosarasinella furcillata* StZ in the Tamri section. For this author, this subzone "falls into an erosional hiatus at least in the west" of the studied

area. This author also noted that the interval between the assemblages of the *N. peregrinus* StSz and *C. furcillata* StZ is always rather thin, even in expanded sections, suggesting "a more or less significant non-sequence all over the study area".

The *Criosarasinella furcillata* Standard Zone; the *C. furcillata* and *Teschenicera callidiscum* standard subzones. The base of the *C. furcillata* StZ is defined by the FAD of the index-species but it can be identified by the FO of *Criosarasinella* (Reboulet, 1996; Reboulet and Atrops, 1999), as made for three studied sections of the present work (Figs. 3–5; FO in ZA52d, AH96 and ZS60). In the Aït Hamouch and Obbay sections (Figs. 4, 8), *Criosarasinella mandovi* was also observed. In the western High Atlas, these both species were recorded by Wippich (2001; 2003) and Ettachfini (2004). The *C. furcillata* StZ is relatively well characterized by the occurrence of *Teschenicera subflucticulum*, *Teschenicera subpachydicranum*, *Neocomites praediscus*? and/or *Olcostephanus densicostatus*. When *Criosarasinella* is absent or rare, as in the Ida w Iddar and Obbay sections (Figs. 7–8), the base of the zone can be placed using the FO of *Teschenicera* (IW41 and OB29). At Aït Hamouch, Zaouia Sidi Abderahmane and Ida w Iddar (Figs. 4–5, 7), the occurrence of *N. praediscus*? may characterize the C. *furcillata* StSz (for the range of these latter taxa, see Reboulet, 1996; Reboulet and Atrops, 1999). In some sections, *Lytoceras subfimbriatum* and *Neolissoceras grasianum* were also recorded; the last specimens of *Bochianites* (probably *Bochianites neocomiensis*) are found in this zone (Figs. 3–5). These three latter taxa were not observed in the lower Valanginian. The *T. callidiscum* StSz was identified in the Zalidou, Aït Hamouch and Zaouia Sidi Abderahmane sections (ZA55, AH102 and AtH15, ZS67, Figs. 3–5). In the latter section, *Teschenicera castellanensiforme* was also sampled at the base of the subzone.

The *Acanthodiscus radiatus* Standard Zone – Base of the Hauterivian stage. The base of the zone is defined by the FAD of the genus *Acanthodiscus*; this marker defines the base of

524 the Hauterivian stage (Mutterlose et al., 2020). In the Aït Hamouch (AH103) and Zaouia Sidi
525 Abderahmane (ZS69) sections, the FO of *A. radiatus* and/or *Acanthodiscus vaceki* is used to
526 place the lower boundary of the Hauterivian (Figs. 4–5). Where these species are absent, the
527 FO *Breistrofferella castellanensis* has been considered in the Zalidou (ZA56) and Aït
528 Hamouch (AtH17) sections (Figs. 3–4). In the three sections (Figs. 3–5), the occurrence of
529 *Teschenicerasflucticulum* and *Tescheniceras pachydicranum* allows to characterize the zone.
530 *Oosterella cultrata* (Aït Hamouch, AtH18) and *Olcostephanus densicostatus* complete the
531 assemblage of the basal part of the Hauterivian in the Aït Hamouch (AH103) and Zaoui Sidi
532 Abderahmane (ZS69) sections. In both sections, few poorly preserved ammonites were found
533 in layers AH103 and ZS70. These specimens might correspond to *T. callidiscum*? but there is
534 no clear evidence that they were reworked from underlying levels. Alternatively, these
535 specimens might be identified as *Saynella mucronata*?. This species was recorded by Wippich
536 (2003) in the condensed Tamri section, more precisely in the first layer dated from the *A.*
537 *radiatus* StZ; according to this author, this may indicate a high stratigraphic level within the
538 zone. Thus, if the identification as *S. mucronata* is correct, it seems that only the upper part of
539 the *A. radiatus* StZ is recorded at Ait Hamouch and Zaoui Sidi Abderahmane. However, as
540 noted by Bulot (1995), the representatives of *Saynella* are very rare in Tethyan basins and the
541 range of *S. mucronata* has to be clarified. Even though the *A. radiatus* StZ is partly
542 represented, it may reach a relatively large thickness at Zaoui Sidi Abderahmane as *A. vaceki*,
543 *B. castellanensis* and *T. flucticulum* still occur around 12 m above the Valanginian–
544 Hauterivian boundary.
545 **Standard zonation and chronostratigraphy.** The current work confirms the reproductibility
546 of the Valanginian standard zonation (Reboulet et al., 2018) and the interest of *N. premolicus*
547 (index-species of the *N. premolicus* StSz) to place the base of the Valanginian when "*T.*"
548 *pertransiens* (index-species of the "*T.*" *pertransiens* StZ) is rare or even absent. Taking in

549 account data provided by the present study, *N. subtenuis* and *B. campylotoxus* local subzones
550 could be introduced in the standard zonation in order to subdived the *N. neocomiensiformis*
551 StZ; these first two species are relatively easy to identify, abundant and have a widespread
552 palaeogeographic distribution (see references above). This point might be discussed by the
553 Kilian Group.
554
555 **4.2. Calcareous nannofossil stratigraphy**
556 The NK3A, NK3B and NC4A subzones of Bralower et al. (1995) were identified in Zalidou
557 and Aït Hamouch sections (Figs. 3–4). In the latter section, the NC4B Subzone was
558 additionally identified. The CC3a, CC3b and CC4a subzones of Sissingh (1977) were
559 identified in both sections; and the CC4b Subzone was identified only at Aït Hamouch
560 (Shmeit et al., 2022, this work). Nannofossil markers are illustrated in Appendix E (Fig. E1,
561 Supplementary material). Quantitative data on calcareous nannofossils is provided by Shmeit
562 et al. (2022) and can be found online (Supplementary material at
563 https://doi.org/10.1016/j.marmicro.2022.102134).
564 Detailed biostratigraphic results and interpretations are presented in the current work and not
565 in Shmeit et al. (2022). Although *Calcicalathina oblongata* defines the base of the NK3 Zone,
566 the precise identification of the FO of this species is problematic due to different taxonomic
567 concepts. Its FO is considered to be situated just above the Berriasian–Valanginian boundary
568 (lower part of the "*T.*" *pertransiens*, Duchamp-Alphonse, 2007; Kenjo et al., 2021) or in the
569 lower Valanginian (Aguado et al., 2000). Indeed, Aguado et al. (2000) recognized earlier
570 specimens, called *Calcicalathina praeoblongata*, which occur in the upper Berriasian (*T.*
571 *alpillensis* StSz); these are very similar in morphology to *C. oblongata* but smaller in average
572 size and with a thick wide wall. However, *C. praeoblongata* figured in Aguado et al. (2000)
573 has been considered by other authors to be overgrown specimens of *Rhagodiscus asper* (see

Kenjo et al., 2021). In the present work, small specimens of *C. oblongata* (< 6 µm) with a thin and bright wall have been recognized in the first samples of the two studied sections; however, in these samples, nannofossils are characterized by large overgrowths which makes more difficult the differentiation between these small forms and larger *C. oblongata*. This species was present in both sections from the first studied sample (*T. alpillensis p.p.* StZ, Zalidou section). The LO of *Rucinolithus wisei*, marking the base of the NK3B Subzone, was observed in the lower part of the upper Valanginian in both sections (*N. peregrinus* StZ at Zalidou and Aït Hamouch, respectively; Figs. 3–4). The LO of *Tubodiscus verenae*, defining the base of the NC4 Zone, was observed in the upper part of the upper Valanginian (uppermost *O. nicklesi* StSz) at Zalidou and in the lower part of the upper Valanginian (uppermost *N. peregrinus* StZ) at Aït Hamouch. The FO of *Lithraphidites bollii*, defining the base of the NC4B Subzone, was observed only at Aït Hamouch in the lowermost Hauterivian *p.p.* (lowermost *A. radiatus p.p.* StZ). The FO of *E. windii*, which identifies the base of the CC3b Subzone, was observed in the middle part of the lower Valanginian (*N. neocomiensiformis* StZ, *N. subtenuis* LSz) at Zalidou and Aït Hamouch. The FO of *E. striatus*, identifying the base of the CC4 Zone, was observed around the lower–upper Valanginian boundary (*K. inostranzewi* StZ or *S. verrucosum* StZ according to the ammonite biostratigraphic interpretation) at Zalidou and in the lower part of the upper Valanginian (*N. peregrinus* StZ) at Aït Hamouch. The identification of *Eiffelithus striatus* followed Shmeit et al. (2022), such that coccoliths have the length of their long-axes greater than 6.0 µm and with a relatively wide central area (almost 2/3 or greater of coccolith length).

Secondary nannofossil bioevents were also observed. The FO of *Speetonia colligata* was recorded in the uppermost Berriasian *p.p.* (*T. alpillensis p.p.* StZ, lowermost NK3A and lowermost CC3a subzones) at Zalidou. It was present from the first studied sample at Aït Hamouch. The FO of *Rhagodiscus dekaenelii* was observed in the lowermost Valanginian

599 (lower *N. premolicus* StSz, lowermost NK3A and lower CC3a subzones) at Zalidou. Its FO
600 was recorded slightly later in Aït Hamouch, in the lower Valanginian (upper *N. subtenuis*
601 LSz, lower NK3A Subzone and CC3a/CC3b subzones boundary). The FO of *Haqius peltatus*
602 was observed in the lower Valanginian in both studied sections; in the upper *N. premolicus*
603 StSz (lower NK3A and upper CC3a subzones) at Zalidou, and in the lower *N. premolicus*
604 StSz (lower NK3A and lower CC3a subzones) at Aït Hamouch.
605 At Zalidou, the LO of *R. wisei* is observed in the early upper Valanginian (*N. peregrinus* StZ,
606 *N. peregrinus* StSz, lower CC4a calcareous nannofossil Subzone), and the LO of *T. verenae* is
607 recorded in the uppermost Valanginian (*N. peregrinus* StZ, *O. nicklesi* StSz, upper CC4a
608 Subzone). Accordingly, the NK3B Subzone extends from 22 to 34.8 m (12.8 m thickness;
609 Fig. 3). However, at Aït Hamouch, the NK3B Subzone is considerably reduced, and extends
610 from 38.6 to 39.8 m (1.2 m thickness, Fig. 4). Ammonite biostratigraphy provides additional
611 information such that the *N. peregrinus* StZ is also reduced at Aït Hamouch (~ 7 m) compared
612 with Zalidou (~ 14 m), and the *O. nicklesi* StSz is not recognized at Aït Hamouch (Figs. 3–4).
613 Additionally, there is no lithological evidence of a condensed interval in the upper part of the
614 *N. peregrinus* StZ, where the LOs of *R. wisei* and *T. verenae* have been recognized. This
615 might indicate that a time-interval is missing in Aït Hamouch compared with Zalidou.
616 To synthetize: a sequence of seven nannofossil bioevents has been recognized in the EAB
617 allowing an accurate biostratigraphic framework to be established. They have been correlated
618 with the ammonite zonation. A comparison of this integrated stratigraphy (ammonites and
619 calcareous nannofossils) with other Tethyan basins is shown in the synthetic Figure 9, and is
620 described as follows.
621 **The FO of *S. colligata* is recorded in the upper Berriasian *p.p.* (*T. alpillensis* StZ)**. This
622 event has the same age in other basins: the Subbetic Basin (Spain, Aguado et al., 2000), the
623 Neuquén Basin (Argentina; Bown and Concheyro, 2004), the site 1213 (Shatskey rise, Pacific

Ocean; Bralower et al., 2002) and the southern Carpathians (Romania; Melinte and Mutterlose, 2001).

The FO of *H. peltatus* is recorded in the lowermost Valanginian (*"T." pertransiens* StZ, *N. premolicus* StSz). In site 1213 (Shatskey rise, Pacific Ocean), this species first occurs in the lower Berriasian (Bralower et al., 2002), i.e. earlier than in the EAB. In the Subbetic Basin, the range of *H. peltatus* starts in the latest lower Valanginian (*K. inostranzewi* StZ, *N. platycostatus* StSz; Aguado et al., 2018); it should be noted that their sampling only concerns the upper part of the *N. neocomiensiformis* StZ and the *K. inostranzewi* StZ. The differences in the FO of *H. peltatus* may be partly explained by its sporadic distribution, as it has been observed in the Valanginian of the EAB.

The FO of *E. windii* is recorded in the lower Valanginian (*N. neocomiensiformis* StZ). This is in accordance with observations of Duchamp-Alphonse et al. (2007) in the Vocontian Basin (SE France, Angles section). In this basin, Bergen (1994) recorded this event slightly later, whereas Kenjo et al. (2021) observed the FO of *E. windii* in the lower part of the "*T". pertransiens* StZ. In other basins, the first record of this species is also dated as lower Valanginian: DSDP 535 (Gulf of Mexico; Bergen, 1994), site 1213 (Shatskey rise, Pacific Ocean; Bralower et al., 2002), Neuquén Basin (Argentina; Bown and Concheyro, 2004) and BGS hole 81/43 (southern North Sea; Kessels et al., 2006).

The FO of *E. striatus* is recorded around the lower–upper Valanginian boundary. The age of this event varies according to the geographic locations of the studied sections. It is considered upper Valanginian (former *H. trinodosum* Zone) in the Vocontian Basin (Bergen, 1994; Duchamp-Alphonse et al., 2007), or in the Neuquén Basin (*N. peregrinus* StZ; Bown and Concheyro, 2004), whereas it is uppermost Valanginian in the Boreal Realm (Greenland–Norwegian Seaway; Möller et al., 2015). Moreover, Kessels et al. (2006) recorded the FO of *E. striatus* in the uppermost Valanginian along a N–S transect (BGS hole 81/43 – southern

North Sea, DSDP 638 – northern west Spain and DSDP 535 – western Atlantic). Aguado et al. (2018) already suggested that the distribution of *E. striatus* might be controlled by the palaeogeographic distribution of land masses and by the palaeoceanographic currents.

The LO of *R. wisei* is recorded in the upper Valanginian (*N. peregrinus* StZ). In the Subbetic Basin (SE Spain; Aguado et al., 2018), its LO is recorded in the upper Valanginian, but slightly earlier (*S. verrucosum* StZ) than in the EAB. In the Vocontian Basin, its LO is recorded earlier, at the lower–upper Valanginian transition (Bergen, 1994; Duchamp-Alphonse et al., 2007; Gréselle et al., 2011). Discrepancies in the LO of *R. wisei* may be explained by its scarcity at the top of its range (Aguado et al., 2018).

The LO of *T. verenae* is recorded in the upper Valanginian (*N. peregrinus* StZ, *O. nicklesi* StSz). This bioevent is also observed in a similar stratigraphic interval (*O. nicklesi* StSz) both in the Vocontian Basin (Duchamp-Alphonse et al., 2007; Gréselle et al. 2011) and in the Subbetic Basin (Aguado et al. 2018).

The FO of *L. bollii* is recorded in the lowermost Hauterivian (*A. radiatus* StZ). This event is observed later (*Crioceratites loryi* StZ) in the Vocontian Basin (Duchamp-Alphonse et al., 2007; Mutterlose et al., 2020) than in the EAB.

Among these seven bioevents, three appear synchronous and are reliable for inter-basin correlation: the FOs of *S. colligata* and *E. windii*, and the LO of *T. verenae.*

4.3. Sedimentology and sequence stratigraphy

4.3.1. Sedimentary discontinuities (Figs. 10–11)

Karst. The top of massive limestone beds frequently presents cm- to dm-scale cavities infilled by marly sediment, distinct from the surrounding limestone, that may contain lithoclasts. When the section is visible, cavities usually decrease in size downward and show a random shape. Fossils in the beds may be dissolved and replaced by iron-rich calcite or

dolomite. These features are interpreted to result from emergence periods, which caused dissolution and karstification by meteoric water. Moreover, karstified surfaces are locally bored; boring resulted probably from the activity of lithophagous molluscs of intertidal to very shallow environment, during the subsequent marine transgression.

Corrugated surface. These surfaces are mainly marked by a wavy shape and by reworking of intraclasts in the immediately overlying bed. In the Valanginian succession, they are often observed at the base of thick beds of fine-grained sandstone or of sandy limestone, and also between thin limestone beds and are only marked by the reworking of small-sized intraclasts. These surfaces are interpreted as resulting from the erosion of the underlying bed(s) that can be reworked in the overlying deposits. In the absence of emergence evidence, they are tentatively ascribed to mainly submarine erosion periods.

Limestone to marlstone abrupt lithological change. In the lower part of the studied series, this kind of surface is usually observed at the top of limestone beds and below a marly succession. It is frequently marked with a phosphate enrichment of the limestone bed in the Berriasian units, and is locally associated with a hardground capping the latter. It is interpreted as traducing a sedimentary hiatus that allowed mineralization (P, Fe) of the bed surface.

Marlstone to sandstone abrupt lithological change. In the upper Valanginian–lowermost Hauterivian part of the series, lithological change commonly occurs between underlying marlstone and overlying thick beds of sandstone. In this case, it is interpreted as an erosional surface which allowed sandy particles to be loosened from the underlying strata, and then sorted out and deposited in a shallow marine, moderately energetic environment as deposition resumed. Usually, the importance of erosion and the occurrence of emergence periods cannot be assessed. In one case, however, the lack of biostratigraphic bio(sub-)zones suggests significant erosions during a long-lasting period of subaerial erosion.

699 In the following text, sedimentary discontinuities are labelled from D0 to D8 in stratigraphical
700 order.
701
702 **4.3.2. Overview of the Berriasian carbonate shelf sedimentation** (Figs. 10–12)
703 Only the top of this series is dated as upper Berriasian (*T. alpillensis* StZ). Identification of
704 the sedimentary discontinuities allows to recognize two depositional sequences. Although
705 poorly dated, they are tentatively correlated across the studied sections. The far bases of the
706 successions are not illustrated in Figs 10 and 11 but their petrographic content is described
707 below in order to show the sequential evolution. In the southern sections (Aït Hamouch, Sidi
708 Abderhamane, Zalidou), the base of the succession is made of relatively massive limestone
709 beds with thin marlstone interbeds. There, the presence of thick marlstone interbeds and an
710 open marine fauna (plicatulids, terebratulids, large bivalves) would indicate an outer shelf
711 environment. However, the abundance of oysters and shallow-water sedimentary features
712 (laminations, HCS, epikarsts) rather suggests a shallow, open marine depositional
713 environment. In the northern sections (Igouzoulen, Obbay), this succession seems to correlate
714 with massive limestone beds made of pelloid-rich wackestone to packstone, rich in oysters,
715 pinnids and locally oolites. The occurrence of several karstified surfaces, tidal laminations
716 and local desiccation breccias indicates a very shallow, inner shelf environment.
717 **The first sequence (Be1)** is represented by a marly interval in the southern sections. Its base
718 is marked by an abrupt lithological change, and by accumulations of phosphate and
719 intraclasts. It shows a thinning-, then thickening-upward evolution. Marlstone contain
720 brachiopods, pectinids, other bivalves among which *Trichites* sp., echinoids, serpulids, and
721 locally bryozoans, and belemnites, whereas the bioturbated limestone beds present oysters,
722 pinnids, and locally trigonids. Microfacies analysis of limestone beds reveals wackestone
723 textures rich in echinoids and small benthic foraminifers, among which few agglutinated

foraminifers, associated with bivalves as oysters, brachiopods and ostracods. This sequence is interpreted as a transgressive then prograding succession, in an open marine outer to inner shelf environment, and witnessing a sea level rise with respect to the underlying deposits. In the Igouzoulen section, this sequence overlies a karstified surface and is dominated by massive limestone beds with thinner marlstone interbeds. In the lower part, pinnids, echinoids, terebratulids and serpulids dominate. In the upper part, thick shelled oysters are dominant, associated with echinoids, pectinids, terebratulids, plicatulids, and finally few ammonites, trigonids and wood fragments. In thin sections, wackestone to packstone textures are predominant and contain a rich fauna of benthic foraminifers, among which are agglutinated forms. The uppermost limestone bed is deeply karstified. In the Obbay section, the upper part of the sequence is made of massive limestone beds containing oysters, trigonids and *Trichites* sp., and is affected by repeated karstification.

The second sequence (Be2) consists of alternating limestone beds and marlstone interbeds; its upper part is dated as uppermost Berriasian (*T. alpillensis* StZ). Its base (D0) is an erosional surface in the southern sections and a karstified surface in the northern ones. In the southern sections, the lower three quarters of the sequence shows a thinning upward trend, while the upper quarter is slightly thickening upward. In the lower part, fauna is abundant and is dominated by oysters and terebratulids, associated with echinoids, pectinids, plicatulids, other bivalves, and locally *Trichites* sp. and fish teeth. In the upper part, ammonites and terebratulids are dominant, with oysters, pectinids, other bivalves, serpulids and nautiloids. The uppermost bed of the sequence is marked by the occurrence of pinnids and oyster coquina. Microfacies evolve from base to top, from sandy wackestone/packstone rich in echinoid remnants and small benthic foraminifers associated with calpionellids, brachiopods and scarce bryozoans, to sandy mudstone/wackestone rich in echinoids and bivalves, with subordinate calpionellids, planktic foraminifers, brachiopods and small benthic foraminifers.

749 In the northern sections, the same evolution is observed, but ammonites are abundant
750 throughout the succession, and microfacies (Igouzoulen) are dominated by wackestone rich in
751 echinoids and benthic foraminifers, both small sized and agglutinated. The presence of
752 agglutinated foraminifers suggests a mild oxygen depletion of the shelf (Kuhnt et al., 1996;
753 Kender and Kaminski, 2017).
754 In all sections, the top of the Be2 sequence is marked by an abrupt lithological change, locally
755 marked by a hardground (Obbay). This sequence is interpreted as constituted by a thick
756 retrograding succession, overlain by a thin prograding unit, deposited in a shallow outer shelf
757 environment. The two above described sequences seem to represent the Cap Tefelney Fm of
758 Rey et al. (1986; 1988).
759
760 **4.3.3. Valanginian–lowermost Hauterivian mixed shelf (Figs. 10–12)**
761 As revealed before, the Berriasian–Valanginian boundary is placed immediately above the D1
762 discontinuity. The identification of discontinuity surfaces allowed to identify eight
763 transgressive-regressive sequences. Because of its condensed nature, the Obbay section will
764 be analyzed separately.
765 **The first sequence (Va1)** is a marly series that comprises scattered thin beds of limestone,
766 belonging to the "*T.*". *pertransiens* StZ and *N. subtenuis* LSz. Its top has not been clearly
767 identified in the Zalidou, Obbay and Ida w Iddar sections. It overlies the D1 discontinuity and
768 presents a thick, thinning upward lower part overlain by a thin, thickening upper part. The
769 calcareous lower part of the sequence contains dominantly oysters, pectinids, echinoids and
770 ammonites. In its middle part, predominant ammonites, belemnites, terebratulids and
771 plicatulids, and very local *Trichites* sp. (Aït Hamouch), express a deepening of the
772 depositional environment. Deepest deposition is reached in the most marly part of the
773 sequence where belemnites dominate. The uppermost part of the sequence is marked by a

faunal assemblage similar to that of the lower part, which indicates a shallowing trend. In Aït Hamouch, HCS and scarce vertebrate remains express a shallower environment. The top of the sequence is marked by a discreet erosional surface. In the central sections, microfacies analysis shows the predominance of mudstone to wackestone textures, and dominant echinoids and agglutinated foraminiferas in the lower and middle part of the sequence. In the upper part, wackestone textures become dominant, with abundant echinoids and bivalves, and subordinate agglutinated foraminiferas.

The second sequence (Va2) is a set of marlstone comprising thin limestone beds, ascribed to the lower part of the *B. campylotoxus* LSz. In the southern sections, its base (D2) is an erosional surface, while it has not been recognized in the Obbay and Ida w Idar sections. In Sidi Abderhamane, it shows a clear thinning-, then thickening-upward trend, whereas it shows a homogeneous trend in other sections. The fauna consists of ammonites, belemnites, brachiopods, plicatulids and other bivalves, suggesting an outer shelf depositional environment. In thin sections, a wackestone texture is observed, containing agglutinated foraminifers, brachiopods, echinoids and benthic foraminifers. This sequence is interpreted as deposited in an open marine, outershelf environment. In Aït Hamouch, the presence of abundant oysters and serpulids, together with echinoids and scarce corals indicates a shallower, and maybe a more mesotrophic environment. This is supported by the occurrence of sandy limestone beds showing cross bedding and HCS.

The third sequence (Va3) is a thin series of marlstone with thin limestone beds. Its base (D3) is an erosional surface, and ammonites ascribe to the middle part of the *B. campylotoxus* LSz. In Igouzoulen, it is reduced to a single sandy limestone bed. Where present, the lithological and faunal evolutions are comparable to that of Va2. The interpretation is, therefore, similar.

The fourth sequence (Va4) is only present in the southern sections, where it is dated to the upper part of the *B. campylotoxus* LSz and the *K. inostranzewi* StZ. In the southernmost

799 sections, it begins with a cross-bedded sandy bed that overlies surface D4. In Zalidou, the
800 basal bed (ZA35) is a limestone bearing oysters, ammonites and plicatulids. The overlying
801 marlstones are rich in pelagic fauna (ammonites, locally belemnites), and are themselves
802 overlain by limestone beds rich in benthic fauna. In Zalidou, however, no limestone beds are
803 observed in the upper part of the sequence, which is directly overlain by a thick sandstone bed
804 (ZA40) suggesting that the upper part of the sequences has been eroded during D5. The Va4
805 sequence is interpreted as a new depositional sequence, the maximum depth of deposition
806 reaching an outer shelf environment. In the Obbay section, the Va2 to Va4 sequences are
807 highly condensed (~ 2 m), and are represented by limestone beds with thin marlstone
808 interbeds. Limestones are slightly sandy wackestone containing predominantly phosphate-
809 and iron-rich oolites, associated with small benthic and scarce planktic foraminifers, and few
810 echinoid or bivalve fragments. Nuclei of oolites are frequently phosphate, glauconite or pyrite
811 granules. These features suggest alternating high energy regime leading to condensation and
812 oolites formation, and low energy periods allowing deposition of micrite. In some beds,
813 partial dissolution of oolites, or local packstone texture with iron-rich micrite suggest
814 emergence periods.
815 **The fifth sequence (Va5)** is a mainly marly to sandy succession, which is present in all
816 sections and is dated early upper Valanginian (*S. verrucosum* StZ and *N. peregrinus* StSz). Its
817 base (D5) is either an erosional surface, or a deeply karstified surface (Igouzoulen, Ida w
818 Iddar). This basal discontinuity is directly overlain either by thick sandy beds (mainly to the
819 north: Zalidou, Igouzoulen, Ida w Iddar), or by marlstone. The basal sandy beds contain both
820 pelagic and benthic fauna to the south and west (Zalidou, Igouzoulen) and only benthic fauna
821 to the north–east. The rest of the sequence shows a thinning-upward evolution, locally
822 overlain by a thickening-upward succession. The marly part of the sequence yields a
823 moderately deep outer shelf fauna (few ammonites and belemnites, associated with

824 terebratulids, serpulids and plicatulids), among which the benthic part becomes more
825 abundant upward.
826 **The sixth sequence (Va6)** is only recognized in the Obbay and Zalidou sections. It
827 corresponds to the *O. nicklesi* StSz of the upper Valanginian. In both sections, surface D6 is
828 overlain by a sandstone bed, but erosion is only visible in Zalidou. At the base, the benthic
829 fauna (plicatulids, echinoids, pectinids) indicates a shallow, open marine environment. It is
830 overlain by silty marlstone bearing belemnites, ammonites, serpulids, with some plicatulids
831 and terebratulids, of outer shelf environment. The middle part of the sequene is rich in pyrite
832 (pyritized ammonites in Obbay). In Zalidou, the upper part is a thickening upward succession
833 of silty marlstone and sandstone beds with ammonites and benthic fauna, expressing a
834 shallowing-upward trend. In Obbay, the reduced thickness and the lack of this thickening
835 upward succession suggest an erosion period during the overlying D7 discontinuity. This is
836 supported by the lack of the *O. nicklesi* StSz in most sections, and suggests that major
837 subaerial erosion occurred during discontinuity D7.
838 **The seventh sequence (Va7)** is present in all sections and its ammonite fauna indicates the
839 uppermost Valanginian (*C. furcillata* StSz and *T. callidiscum* StSz). It consists of a mainly
840 marly to sandy succession that overlies an erosional surface (D7). In most sections, D6 and
841 D7 are merged. This basal discontinuity is directly overlain by a sandy bed containing an
842 abundant open marine fauna, among which pectinids, plicatulids and echinoids indicate a
843 shallow environment. This is supported by the local occurrence of wood and leave fragments
844 (Sidi Abderhamane) and probable evaporite pseudomorphs (Ida w Iddar). The middle part of
845 the sequence bears a deep outer shelf fauna (belemnites, ammonites, plicatulids,
846 terebratulids). In the southern sections, no thickening-upward evolution is observed in the
847 upper part of the sequence, whereas the northeastern sections (Zalidou, Ida w Iddar) display
848 clearly the progradation of a clastic system. In the upper part of the sequence, the southern

sections display an outer shelf fauna (plicatulids, belemnites, terebratulids, ammonites), while the Ida w Iddar section is marked by very shallow sedimentary features (HCS, ripple marks, tidal laminations).

Only the lower part of the eighth sequence (Ha1) has been studied. In spite of scarce ammonite fauna, discontinuity D8 seems to roughly coincide with the Valanginian–Hauterivian boundary, since ammonites of the *A. radiatus* StZ are found above (Aït Hamouch, Zaouia Sidi Abderhamane), or immediately below (Zalidou) the surface D8. Ha1 begins with a sandy bed in the southern sections (Aït Hamouch, Sidi Aberhamame), or with sandy marlstone in the northern sections. The rest of the studied succession shows a tinning-upward trend and a scarce outer shelf to pelagic fauna.

4.4. Carbon isotope stratigraphy

The measured $\delta^{13}C_{carb}$ values range between -2.8 and +1 (avg. -0.8 ‰) at Zalidou, -3.3 and +0.4 (avg. -1.5 ‰) at Aït Hamouch, -3.2 and -0.1 (avg. -1.3 ‰) at Zaouia Sidi Abderahmane, -4 and -0.8 (avg. -1.8 ‰) at Igouzoulen, and -4.7 and -0.2 (avg. -1.8 ‰) at Ida w Iddar (Figs. 3–7). The $\delta^{13}C_{carb}$ values of sections are provided in Appendix F (Supplementary material). Among the studied sections in the EAB, Zalidou (Fig. 3) presents the highest sampling resolution and is considered as the reference section for the $\delta^{13}C_{carb}$. The Weissert Event is identified from the base of the CIE, until its climax, following the formal definition of Erba et al. (2004). According to this definition, the CIE is observed at Zalidou from the basal part of *K. inostranzewi* StZ (16.25 m) to the upper part of *O. nicklesi* StSz, in which the climax is recorded at 32.8 m (upper NK3A to upper NK3B and upper CC3b to upper CC4a calcareous nannofossil subzones). Below this peak, there is a short-lived plateau of values comprised between 0 and 1 ‰ (dated from the *O. nicklesi* StSz); above the climax, the isotopic curve is characterized by a slow decrease in values (uppermost *O. nicklesi* StSz and *C. furcillata* StZ).

874 The top of the Weissert Event is recorded just below the LO of the nannofossil biomarker *T.*
875 *verenae*, marking the base of the nannofossil Zone NC4. At Aït Hamouch (Fig. 4), the CIE is
876 cautiously identified from 32.8 (*K. inostranzewi* StZ) to ~36 m (middle part of *N. peregrinus*
877 StZ). In this section, *S. verrucosum* StZ was not recognized separately (see AH89 and
878 comments on ammonite biostratigraphy). Additionally, the *N. peregrinus* StZ is reduced (~ 7
879 m) compared with Zalidou (~ 14 m), and the *O. nicklesi* StSz was not recognized. This can be
880 also observed from the reduced NK3B calcareous nannofossil Subzone in Aït Hamouch (1.2
881 m) compared with Zalidou (12.8 m). The slow decrease of $\delta^{13}C_{carb}$ values in the *C. furcillata*
882 StZ is recorded. At Zaouia Sidi Abderahmane (Fig. 5), the CIE starts in the upper part of the
883 *K. inostranzewi* StZ (~ 30 m) and the climax value is recorded in the *N. peregrinus* StZ (~
884 34.5 m). After this peak, the decrease of the values is mainly observed in the *C. furcillata* StZ.
885 Again, the plateau phase of positive $\delta^{13}C_{carb}$ values is not recognized before the climax. At
886 Igouzoulen (Fig. 6), it is difficult to recognize the CIE; it could be placed between 36 and 40
887 m (*K. inostranzewi* StZ and *S. verrucosum* StZ). At Ida w Iddar (Fig. 7), the CIE could be
888 placed between 12 and 16 m (*K. inostranzewi* StZ and *N. peregrinus* StZ). It should be noted
889 that the *C. furcillata* StZ is also characterized by a smooth decrease of $\delta^{13}C_{carb}$ values. To
890 summarize, the plateau phase of positive $\delta^{13}C_{carb}$ values below the climax is only recognized
891 in the Zalidou section and is dated to the *O. nicklesi* StSz. This interval may be missing in the
892 other sections due to a strong erosion expressed by the sedimentary discontinuities (D6-D7
893 merged; Figs. 4–5, 7).
894
895 **5. Discussion**
896 The detailed zonations based on ammonite and calcareous nannofossil data allow to date
897 accurately the significant changes in $\delta^{13}C_{carb}$ values and to ascribe an age for the sedimentary
898 discontinuities observed in the EAB. This integrated zonal scheme supports detailed

899 correlations of these events with those recorded in other basins of the northern Tethyan
900 margin, for which integrated stratigraphic studies were also made. In the following parts,
901 comparisons are mainly proposed with SE France and occasionally with other areas.

902 **5.1. Inter-basin correlation of carbon isotopic events**

903 The Weissert Event recorded in the EAB is here compared with carbon isotope data available
904 in SE France, only if constrained by ammonite and nannofossil biostratigraphy (Hennig et al.,
905 1999; Duchamp-Alphonse et al., 2007; McArthur et al., 2007; Gréselle et al., 2011; Kujau et
906 al., 2012; Martinez et al., 2013; 2015; Gollain et al., 2019). For the "*T.*" *pertransiens* StZ and
907 the lower part of the *N. neocomiensiformis* StZ, the carbon isotope data of the Angles section
908 (Valanginian hypostratotype, SE France; Duchamp-Alphonse et al., 2007) were added on the
909 Vergol-La Charce composite section representing the Vocontian Basin succession (Fig. 13).
910 This part of the curve (dashed line) must be interpreted carefully as it is challenging to
911 establish correlations between the Vergol-La Charce and Angles sections. The log of the
912 Angles section given by Duchamp-Alphonse et al. (2007) is not detailed, and the lower
913 Valanginian ammonite zonal scheme was not improved since Busnardo and Thieuloy (1979;
914 see Bulot and Thieuloy, 1995).
915 A slight decrease in $\delta^{13}C_{carb}$ values (around -0.5 ‰) is observed from the lower part of "*T.*"
916 *pertransiens* StZ to the lower part of *N. neocomiensiformis* StZ; an increase of a same order is
917 recorded in the upper part of this zone. A similar trend (with a stronger amplitude, around +/-
918 1 ‰) is recorded in some sections of the EAB as Ait Hamouch and Zaouia Sidi Abderahmane
919 (Figs. 4–5). In SE France (Gréselle et al., 2011; Martinez et al., 2015; Gollain et al., 2019;
920 Fig. 13) and SE Spain (Aguado et al., 2018), detailed biostratigraphic data show that the onset
921 of the CIE occurs in the *K. inostranzewi* StZ, more precisely below the boundary between *K.*
922 *inostranzewi* StSz and *N. platycostatus* StSz (lowest values of $\delta^{13}C$; 0.14‰ and 0.1‰,
923 respectively). In the *K. inostranzewi* StSz, the pre-CIE $\delta^{13}C$ curve shows oscillations between

924 0.4‰ and 1‰. In the Vocontian Basin, the basal part of this subzone is characterized by four
925 organic-matter-rich layers (Barrande layers; Reboulet et al., 2003) that are not observed in the
926 studied Moroccan area. In some sections of the EAB, low $\delta^{13}C_{carb}$ values are recorded in the
927 *K. inostranzewi* StZ and were interpreted as the onset of the CIE (Aït Hamouch and Zaouia
928 Sidi Abderahmane; Figs. 4–5). At Zalidou, two negative peaks are observed in the *K.*
929 *inostranzewi* StZ (Figs. 3, 13). The first one (-2.7‰), located at the base, is followed by an
930 increase of isotopic values that continues until the lower part of the *N. peregrinus* StZ. A
931 single point, located at the top of the *K. inostranzewi* StZ, is clearly outside of this curve
932 trend. As it is the lowest value recorded in the Zalidou section (-2.8‰), this might correspond
933 to the onset of the CIE. This would be in agreement with observations made on the Aït
934 Hamouch and Zaouia Sidi Abderahmane sections, for which the CIE starts in the interval
935 between discontinuities D4 and D5 (Figs. 4–5). However, as the onset of the CIE occurs only
936 few meters above the SB F defined by Gréselle and Pittet (2010) in the Vocontian Basin (Fig.
937 13), the isotopic event may start with D4 (or close to this discontinuity) at Zalidou. As a
938 matter of fact, part of the time recorded by deposits in the deep Vocontian Basin is most
939 probably lacking in the EAB, where D4 corresponds to a major emergence surface, on which
940 sedimentation resumed later than in the Vocontian Basin. This interpretation is consistent with
941 the calcareous nannofossils data at Aït Hamouch and Zalidou, which show that the beginning
942 of the Weissert Event is characterized by the FO of *H. circumradiatus* and by a decrease in
943 the nannoplankton production (Shmeit et al., 2022). Consequently, the onset of the CIE at
944 Zalidou may be placed at the first negative shift in $\delta^{13}C_{carb}$ values (-2.7‰), i.e. at the base of
945 the *K. inostranzewi* StZ (Fig. 3). Diagenetic impacts on platform carbonates during emergence
946 periods and meteoritic diagenesis (Godet et al., 2016) may explain the strong negative values
947 observed just below D5 at Zalidou ($\delta^{13}C_{carb}$ = -2.8‰), as well as immediately below D8 at Ait
948 Hamouch ($\delta^{13}C_{carb}$ = -5.9‰; Fig. 13).

In the Vocontian Basin, the maximum of $\delta^{13}C_{carb}$ values is recorded in the *S. verrucosum* StZ (double peaks in the *S. verrucosum* StSz; Duchamp-Alphonse et al., 2007; McArthur et al. 2007; Kujau et al., 2012; Martinez et al., 2015; Gollain et al., 2019). This trend in the isotopic curve is not recorded in the EAB. It can be partly explained by condensed intervals and/or stratigraphic gaps around the lower–upper Valanginian boundary; the *S. verrucosum* StZ was partly (Zalidou, Zaouia Sidi Abderahamane) or not (Aït Hamouch; see AH89 and comments on ammonite biostratigraphy) recognized. In these Moroccan sections, the maximal values are observed in the *N. peregrinus* StZ and may correspond to the plateau of high values recorded in the *N. peregrinus* StZ in SE France (Martinez et al., 2015; Fig. 13) and SE Spain (Aguado et al., 2018). In both latter areas, as in the EAB, the carbon isotope curve is characterized by a slow decrease of $\delta^{13}C_{carb}$ values that starts in the uppermost part of the *N. peregrinus* StZ (Ait Hamouch and Zaouia Sidi Abderrahmane), more precisely at the top part of the *O. nicklesi* StSz (Zalidou), and continues in the *C. furcillata* StZ (Zalidou, Ait Hamouch, Zaouia Sidi Abderrahmane, and Ida w Iddar sections; Figs. 3–5, 7). Thus, except for the interval corresponding to the *S. verrucosum* StZ, the main trends of the Valanginian carbon isotope curve in the northern Tethyan basins are similarly observed in the EAB.

5.2. Inter-basin correlation of discontinuities

The EAB is correlated mainly with the SE France Basin, for which biostratigraphic, isotopic and sedimentologic data are all available and a platform-basin transect for the Valanginian depositional system was already established (Arnaud et al., 1981; Reboulet, 1996; Gréselle and Pittet, 2010 and references therein). Thus, the French and Moroccan basins are relevant areas to illustrate the North and South Tethyan margins, respectively.

In the northern Vocontian Basin, Gréselle and Pittet (2010) identified five major sequence boundaries in the Valanginian succession. Their discontinuity “D”, at the Berriasian–

974 Valanginian boundary (lowermost part of the "*T.*" *pertransiens* StZ *sensu* Kenjo et al., 2021),
975 corresponds to our SB D1. This discontinuity seems largely identified in SE France, since a
976 basal Valanginian discontinuity (between their "*Thurmanniceras" otopeta* (sub-)zone and
977 "*T.*" *pertansiens* ammonite zone) has been identified in the Subalpine chain by Arnaud et al.
978 (1981; their D-VI) and Morales et al. (2013; their SBe), and in the Provence Platform (DCB
979 of Bulot et al., 1995; 1997). Like in the EAB, these surfaces separate the underlying carbonate
980 shelf from overlying marlstone and limestone, locally sandy. Discontinuity "E" (Gréselle and
981 Pittet, 2010), ascribed to the lower part of the *N. neocomiensiformis* StZ, likely correlates with
982 D-VII of Arnaud et al. (1981), SBf of Morales et al. (2013) and D2 of this work.
983 Discontinuity D3 of the EAB, ascribed to the upper part of the *N. neocomiensiformis* StZ
984 (middle part of the *B. campylotoxus* LSz) may be correlated with the minor discontinuity
985 placed by Gréselle and Pittet (2010, their fig. 14) between their V4 and V5 sequences.
986 In SE France, the interval around the lower–upper Valanginian boundary is marked by two
987 successive discontinuities: D-VIII and D-IX of Arnaud et al. (1981). According to their
988 correlations with the Angles section (fig. 6 of Arnaud et al., 1981) and according to the
989 standard zonation used here in the Vocontian Basin composite section (Fig. 13), D-VIII and
990 D-IX may correspond to the basal (SB F) and top discontinuities of sequence V6 in Gréselle
991 and Pittet (2010), ascribed to the basal parts of the *K. inostranzewi* StZ and *S. verrucosum*
992 StZ, respectively. According to Bulot (1995, p. 246; see also Bulot et al., 1997), the mid–
993 Valanginian discontinuity of Masse and Lesbros (1987; "discontinuité médiovalanginienne")
994 and the discontinuity of the middle Valanginian (DVM *sensu* Autran, 1993), dated to the
995 basal and top parts of the *K. inostranzewi* zone, respectively, are distinct, contrary to the
996 suggestion of Autran (1993), who correlated them. This discrepancy in interpretations may be
997 due to the very shallow depositional environments at that time, and correlative emergence
998 periods, subsequent erosion and/or amalgamation of discontinuity surfaces (Arnaud et al.,

1981; Masse and Lesbros, 1987; Autran, 1993; Bulot, 1995; Bulot et al., 1995; 1997; 2010; Gréselle and Pittet, 2010; Morales et al., 2013), as observed in the Moroccan studied area. In the EAB, as D4 is ascribed to the *K. inostranzewi* StZ in the Zalidou (Fig. 13), Zaouia Sidi Abderahmane and Obbay sections, this discontinuity may be correlated with D-VIII of Arnaud et al. (1981) and with discontinuity "F" of Gréselle and Pittet (2010). In both areas, this discontinuity marks a major facies change, corresponds to the shallowest part of the succession and is unconformable onto previous deposits. D4 may correspond to the "discontinuité médiovalanginienne" of Masse and Lesbros (1987). As observed in the Aït Hamouch and Zaouia Sidi Abderahmane sections (see previous explanations for Zalidou) and in SE France (Vocontian Basin and Provence Platform; Fig. 13), D4 and SB F, respectively, are followed by a negative shift in $\delta^{13}C_{carb}$ values corresponding to the onset of the CIE. Discontinuity D5 caps a depositional sequence that onlaps onto the D4 major discontinuity and thus wedges out eastward (Fig. 12), while D4 is merged with D5 in the Igouzoulen and Ida w Iddar sections of the EAB (Fig. 11). D5 is identified at the lower–upper Valanginian boundary (*K. inostranzewi* StZ–*S. verrucosum* StZ boundary) in the Zalidou, Ida w Iddar and Obbay sections (Figs. 3, 7–8); this discontinuity is ascribed to the basal part of the *S. verrucosum* StZ at Zaouia Sidi Abderahmane and Igouzoulen (Figs. 5–6). Therefore, D5 should be correlated with D-IX of Arnaud et al. (1981), the DVM of Autran (1993) and with the minor SB that separates V6 and V7 sequences of Gréselle and Pittet (2010).

In the EAB, where overlain by the Va6 sequence, D6 occurred in the top part of the *N. peregrinus* StSz at Zalidou and Obbay sections (Figs. 3, 8), where the *O. nicklesi* StSz was recognized. In successions of the Vocontian Basin, Reboulet et al. (1992) mentioned a SB that underlines Lowstand deposits ("Faisceau median" or "Peregrinus bundle", La Charce section) dated to the *N. peregrinus* StSz (Reboulet and Atrops, 1999), while Gréselle and Pittet (2010)

identified their discontinuity G also in the lower part of the same (Sub-)zone. Therefore, these events likely correlate with the D6 of the EAB (Fig. 13).

In SE France, Autran (1993) identified a major discontinuity in the upper Valanginian, namely the upper Valanginian discontinuity (DVS), ascribed by this author to the former *H. trinodosum* Zone (equivalent to the *O. nicklesi* StSz and *C. furcillata* StSz). According to biostratigraphic data provided by Reboulet (1996), the DVS occurs at the *N. peregrinus* StZ–*C. furcillata* StZ boundary. Consequently, this discontinuity may be correlated with our D7 since the latter is also situated between these standard zones (Zalidou and Obbay sections). The D7 is responsible for the partial or total erosion of our Va6 depositional sequence and is frequently merged with D6 (Figs. 9–10). Consistently, the DVS is associated in SE France with erosions that may remove down to the middle Valanginian discontinuity *sensu* Autran (1993; DVM). Studying basinal successions, Reboulet et al. (1992) defined a SB discontinuity at the base of thick Lowstand deposits (Furcillata calcareous bundle in Fig. 13) encompassing the upper part of the *O. nicklesi* StSz and the lower part of the *C. furcillata* StSz. Since there are probably no Lowstand deposits in the EAB, the SB of Reboulet et al. (1992) likely correlates with the D7 of the EAB. It also correlates with discontinuity H of Gréselle and Pittet (2010), placed at the top of the *O. nicklesi* StSz. Nevertheless, the latter authors interpret the D5–D7 interval as a period of sea level fall following a major transgression, whereas we interpret the same interval in the EAB as a transgressive–regressive cycle, the maximum flooding of which is placed in the *O. nicklesi* StSz.

In the EAB, D8 is placed at the Valanginian–Hauterivian boundary (Aït Hamouch and Zaouia Sidi Abderahmane; Figs. 4–5) or in the lowermost part of the lower Hauterivian *A. radiatus* StZ (Zalidou, Fig. 3). This discontinuity corresponds to a strong regression. It correlates, in SE France (Fig. 13), with the major surface D-X of Arnaud et al. (1981), with the base of Lowstand deposits of Reboulet et al. (1992), with the top of the V12 sequence of Gréselle and

1048 Pittet (2010), and with the uppermost Valanginian discontinuity (DVT of Bulot et al., 2010;
1049 see also Reboulet, 1996, p. 275). In SE France, this discontinuity corresponds to a hiatus in
1050 shelf areas and may comprise several surfaces (Bulot et al., 2010).
1051
1052 **5.3. Sea level changes and sequence origin**
1053 The comparisons exposed above show that most of the discontinuities identified in the EAB
1054 are also known elsewhere, especially in SE France. This strongly suggests that eustacy
1055 controlled the evolution of both areas. Following the two Berriasian sequences, which express
1056 a transgressive trend with respect to the base of the sections, the Valanginian succession can
1057 be divided into three main transgressive–regressive cycles, divided by the main
1058 discontinuities D4 and D7 (Fig. 12). The first one includes Va1 to Va3, the second one
1059 comprises Va4 to Va6, and the third one is made of the Va7 sequence. The maximum
1060 flooding of the first cycle occurred during the lower part of the *N. neocomiensiformis* Stz,
1061 namely the *N. subtenuis* LSz; the maximum depositional depth of the second cycle seems to
1062 be reached in the *O. nicklesi* StSz, and a third maximum flooding is reached during the *C.*
1063 *furcillata* StSz.
1064 The Va2 and Va3 sequences encompass a period of low sea level (Haq, 2014), which
1065 culminates with the major D4 discontinuity. The latter is marked by deeply karstified surfaces
1066 amalgamating several discontinuities in the proximal northern sections and is overlain by the
1067 Va4 sequence that onlaps toward the north or northeast. In the southern part of the EAB, the
1068 "mid–Valanginian events" of Masse and Lesbros (1987) are represented by at least three
1069 discontinuities, materialized by erosional surfaces in the southern sections. These
1070 discontinuities bound depositional sequences marked by an open marine fauna indicating an
1071 outer shelf environment, which suggests that sea level oscillations were of high amplitude.
1072 Moreover, in the Aït Hamouch section, the Va2, Va3, and part of the Va4 sequences belong to

1073 the *B. campylotoxus* LSz. According to Martinez et al. (2013), the duration of the *B.*
1074 *campylotoxus* subzone is estimated at 390 ky. Since their work, the conception of some zones
1075 or sub-zones has changed for the upper part of the lower Valanginian with the introduction of
1076 the *N. neocomiensiformis* StZ and *K. inostranzewi* StZ (Reboulet et al., 2014, p. 128–129 and
1077 tab. 2). Accordingly, the conception of the *B. campylotoxus* LSz used in the EAB sections
1078 would correspond to a larger stratigraphic interval in the Vergol section (Vocontian Basin)
1079 than considered in the work of Martinez et al. (2013). Consequently, the duration of the
1080 Moroccan *B. campylotoxus* LSz would be higher than 390 ky and may be estimated at around
1081 570 ky. This means that the average duration of the sequences identified in the Aït Hamouch
1082 section is around 200 ky. Although not conclusive, these observations are consistent with an
1083 orbitally-driven, glacio-eustatic origin for these rapid and high amplitude sea level
1084 fluctuations, as suggested for the "middle Valanginian" (Price, 1999; Gréselle and Pitet, 2010;
1085 Martinez et al., 2013; Charbonnier et al., 2020).
1086 As a whole, the second and third cycles present deeper depositional environments than the
1087 first one, expressing a rise in sea level, likely responsible for the drowning of the lower
1088 Valanginian carbonate shelf in the EAB, as well as around the world (Föllmi, 2012).
1089 Additionally, the upper Valanginian deposits are more clayey than the lower Valanginian first
1090 cycle, suggesting an increase of terrigenous supply. Such change has been observed elsewhere
1091 in the world, and interpreted as a change toward more humid conditions (e.g., Schlager, 1980;
1092 Bulot et al., 1997; Föllmi, 2012; Bottini et al., 2018).
1093 In SE France, Masse and Lesbros (1987) noted that what they call the "mid–Valanginian
1094 events" are associated with a sharp deepening of the depositional environments and with the
1095 development of gravitationally reworked sediments, as well as significant terrigenous input
1096 (Duchamp-Alphonse et al., 2007). They propose, therefore, that the area was submitted to
1097 tectonic movements of the basement (Masse and Lesbros, 1987; Bulot et al., 1997). A partly

tectonic origin has also been suggested for the major discontinuity observed around the lower–upper Valanginian boundary in Argentina (Schwarz and Buatois, 2012), and although less accurately dated, in Romania (Gradinaru et al., 2016), and Sardinia (Bottini et al., 2018). In the EAB, neither synsedimentary deformation features nor sharp subsidence changes have been observed around the lower–upper Valanginian boundary. However, as in SE France, the upper Valanginian deposits are marked by a significantly higher amount of terrigenous sediments (sand and silt), especially in the northeastern sections (Fig. 12). This may indicate an erosion resumption in the present-day High Atlas, which may have been triggered by tectonic movements. Nevertheless, since most of the discontinuities identified in the EAB are also known in other areas of the world, these possible tectonic movements were mild enough not to disturb the eustatic signal.

6. Conclusion

The integrated study (ammonites, calcareous nannofossils, sedimentology, sequence stratigraphy, carbon isotopes) of the upper Berriasian–lowermost Hauterivian interval along six sections (Zalidou, Aït Hamouch, Zaouia Sidi Abderahmane, Igouzoulen, Ida w Iddar and Obbay) located in the Essaouira-Agadir Basin (Morocco, South Tethyan margin) led to the following major results.

1. A systematic revision of the whole ammonite fauna was made and the stratigraphic distributions of taxa are given for all studied sections. The analysis of their ranges allowed the establishment of a detailed zonal scheme, more particularly for the lower Valanginian. It corresponds to the standard zonation (Reboulet et al., 2018) for the Mediterranean Province of the Mediterranean–Caucasian Subrealm (Tethyan Realm). Two local subzones were added in the *Neocomites neocomiensiformis* Standard Zone, which is recognized for the first time in the Moroccan lower Valanginian successions. The base of the Valanginian and that of the

upper Valanginian are placed at the base of the "*Thurmanniceras*" *pertransiens* Standard Zone and that of *Saynoceras verrucosum* Standard Zone, respectively.

2. A calcareous nannofossil biostratigraphy was established in the most suitable sections (Zalidou and Aït Hamouch) for nannofossil studies (Shmeit et al., 2022; this work). The calcareous nannofossil zonal schemes of Sissingh (1977) and Bralower et al. (1995) are recognized, and a sequence of seven nannofossil bioevents is identified. Thus, ammonite and nannofossil zonations are calibrated for these reference sections.

3. Detailed sedimentological field and microfacies analysis, led to recognize sedimentary discontinuities (D0 to D8), which allowed a sequence stratigraphic analysis of the basin. Two depositional sequences are recognized in the Berriasian (Be1 and Be2), seven in the Valanginian (Va1 to Va7) and one in the Hauterivian (Ha1). Major discontinuities resulted in significant erosions that led locally to amalgamated surfaces, at the lower–upper Valanginian boundary interval (D4–D5) and in the middle part of the upper Valanginian (D6–D7).

4. Carbon isotope analyses were made in five sections. The Weissert Event is well recorded in the highest resolution $\delta^{13}C_{carb}$ curve obtained in this study (Zalidou). The mid–Valanginian carbon isotope excursion is also relatively well observed at Aït Hamouch and Zaouia Sidi Abderahmane, but more cautiously interpreted elsewhere. The precise age of its onset is obscured by the major "mid–Valanginian" eustatic regression that led to a widespread emergence, erosions, and sedimentary hiatuses (D4–D5).

5. The Valanginian carbon isotope record observed in the Essaouira-Agadir Basin is similar to those recorded in the south–east France Basin. The Moroccan sedimentary discontinuities can be correlated with those identified in south–east France, suggesting that eustacy mainly controlled the evolution of both depositional areas.

Acknowledgements

Our project on the Essaouira-Agadir Basin benefited of financial supports from a project (2013–2015) funded by the Moroccan and French Ministries of foreign affairs (Partenariat Hubert Curien, Volubilis n° 031/STU/13), from the French IRD, Campus France, and various grants from ISTerre, the Laboratoire de Géologie de Lyon, the OSUG@2020 Labex, the CNRS SYSTER program and IODP France soutien post-cruise. Christophe Despierres (Grenoble) and Thomas Letulle (Lyon) are thanked for their contribution to this study through Master memoirs. We acknowledge Emmanuel Robert (University of Lyon) for help in completing the macrofossil sampling in some sections. We are indebted to Mohssine Ettachfini (University of Marrakech, Morocco), who gave full access to his ammonite collections and made helpful suggestions. We are extremely grateful to Miguel Company (University of Granada, Spain) for fruitful discussions on ammonites. We are grateful to the editor Eduardo Koutsoukos, Beatriz Aguirre-Urreta and an anonymous reviewer for both corrections and comments which greatly improved the quality of an earlier version of the manuscript.

References

Aguado, R, Company, M., Castro, J.M., de Gea, G.A., Molina, J.M., Nieto, L.M., Ruiz-Ortiz, P.A., 2018. A new record of theWeissert episode from the Valanginian succession of Cehegín (Subbetic, SE Spain): Bio- and carbon isotope stratigraphy. Cretaceous Research 92, 122–137.

Aguado, R, Company, M., Tavera, J.M., 2000. The Berriasian/Valanginian boundary in the Mediterranean region: new data from the Caravaca and Cehegín sections, SE Spain. Cretaceous Research 21, 1–21.

1172 Aguirre-Urreta, M.B., Alvarez, P.P., 1999. The Berriasian genus *Groebericeras* in Argentina
1173 and the problem of its age. Scripta Geologica Special Issue 3, 15–29.
1174 Aguirre-Urreta, B., Martinez, M., Schmitz, M., Lescano, M., Omarini, J., Tunik, M., Kuhnert,
1175 H., Concheyro, A., Rawson, P.F., Ramos, V.A., Reboulet, S., Noclin, N., Frederichs, T.,
1176 Nickl, A.-L., Pälike, H., 2019. Interhemispheric radio-astrochronological calibration of the
1177 time scales from the Andean and the Tethyan areas in the Valanginian–Hauterivian (Early
1178 Cretaceous). Gondwana Research 70, 104–132.
1179 Algouti, A., Algouti, A., Taj-Eddine, K., 1999. Le Sénonien du Haut Atlas occidental,
1180 Maroc : sédimentologie, analyse séquentielle et paléogéographie. Journal of African Earth
1181 Sciences 29, 643–658.
1182 Ambroggi, R., 1963. Etude géologique du versant méridional du Haut Atlas occidental et de
1183 la plaine du Souss. Notes du Service géologique du Maroc 157, 322 pp.
1184 Applegate, J.L., Bergen, J.A., 1988. Cretaceous calcareous nannofossiil biostratigraphy of
1185 sediments recovered from the Galicia margin, ODP Leg 103. Proc. In: Boillot, G.,
1186 Winterer, E. L., et al. (Eds), Proceedings of the Ocean Drilling Program, Scientific Results
1187 103, College Station, TX (Ocean Drilling Program), 293–348.
1188 Arnaud, H., Gidon, M., Thieuloy, J.-P., 1981. Les Calcaires du Fontanil des environs de
1189 Grenoble : leur place dans la stratigraphie du Néocomien entre le Jura et le domaine
1190 vocontien. Eclogae Geologicae Helvetiae 74, 109–137.
1191 Autran, G., 1993. L'évolution de la marge nord-est provençale (Arc de Castellane) du
1192 Valanginien moyen à l'Hauterivien à travers l'analyse biostratigraphique des séries de la
1193 région de Peyroules : séries condensées, discontinuités et indices d'une tectogenèse
1194 distensive. Paléobiologie. Annales du Muséum d'Histoire Naturelle de Nice 10, 240 pp.

1195 Ben Ammar, S., Layeb, M., 2021. Updated geochemical insights on the Weissert and Faraoni
1196 events in the southern Tethyan margin (northern Tunisia). Arabian Journal of Geosciences
1197 14, 2379.
1198 Bergen, J.A., 1994. Berriasian to early Aptian calcareous nannofossils from the Vocontian
1199 trough (SE France and deep sea drilling site 534: new nannofossil taxa and a summary of
1200 low-latitude biostratigraphic events. Journal of Nannoplankton Research 16, 59–69.
1201 Blanc, E., Bulot, L.G., Paicheler, J.C., 1994. La coupe de référence de Montbrun-les-Bains
1202 (Drôme, SE France) : un stratotype potentiel pour la limite Berriasien–Valanginien.
1203 Comptes Rendus de l'Académie des Sciences de Paris 318 (sér. II), 101–108.
1204 Bottini, C., Dieni, I., Erba, E., Massari, F., Weissert, H., 2018. The Valanginian Weissert
1205 oceanic anoxic event recorded in central-eastern Sardinia (Italy). Rivista Italiana di
1206 Paleontologia e Stratigrafia 124(3), 617–637.
1207 Bouatmani, R., Chakor Alimi, A., Medina, F., 2007. Subsidence, évolution thermique et
1208 maturation des hydrocarbures dans le bassin d'Essaouira (Maroc) : apport de la
1209 modélisation. Bulletin de l'Institut Scientifique Rabat 29, 15–36.
1210 Bourgeoini, Y., Ali Nabiha, B.H., Saloua, R., Kamal, T., 2002. Etude biostratigraphique du
1211 Crétacé inférieur (Barrémien supérieur-Albien) du Haut Atlas Occidental (Maroc).
1212 Estudios Geológicos 58, 109–116.
1213 Bown, P.R., Concheyro, A., 2004. Lower Cretaceous calcareous nannoplankton from the
1214 Neuquén Basin, Argentina. Marine Micropaleontology 52, 51–84.
1215 Bralower, T.J., 1987. Valanginian to Aptian calcareous nannofossil stratigraphy and
1216 correlation with the upper M-sequence magnetic anomalies. Marine Micropaleontology 11,
1217 293–310.
1218 Bralower, T.J., Leckie, R.M., Sliter, W. V., Thierstein, H.R., 1995. An Integrated Cretaceous
1219 Microfossil Biostratigraphy. Geochronology Time Scales and Global Stratigraphic

1220 Correlation. Society of Economic Paleontologists and Mineralogists Special Publication
1221 54, 65–79.
1222 Bralower, T.J., Monechi, S., Thierstein, H.R., 1989. Calcareous nannofossil zonation of the
1223 Jurassic-Cretaceous boundary interval and correlation with the geomagnetic polarity
1224 timescale. Marine Micropaleontology 14, 153–235.
1225 Bralower, T.J., Premoli Silva, I., Malone, M.J., 2002. Shipboard Scientific Party, 2002. Site
1226 1213. In: Bralower, T.J., Premoli Silva, I., Malone, M.J., et al., Proceedings of the Ocean
1227 Drilling Project, Initial Reports 198, 1–110.
1228 Bulot, L.G., 1995. Les formations à ammonites du Crétacé inférieur dans le Sud-Est de la
1229 France (Berriasien à Hauterivien) : biostratigraphie, paléontologie et cycles sédimentaires.
1230 Unpublished PhD thesis, Muséum National d'Histoire Naturelle, Paris, 398 pp.
1231 Bulot, L.G., Thieuloy, J.-P., 1995. Les biohorizons du Valanginien du Sud-Est de la France : un
1232 outil fondamental pour les corrélations au sein de la Téthys occidentale. Géologie Alpine,
1233 Mémoire Hors Série 20 (1994), 15–41.
1234 Bulot, L.G., Masse, J.-P., Moutier, L., Virgonne, A., 1997. Organisation stratigraphique et
1235 dynamique sédimentaire du Valanginien au passage plate-forme/bassin en Basse-Provence
1236 (S-E France). Bulletin de la Société géologique de France 168, 171–179.
1237 Bulot, L.G., Thieuloy, J.-P., Arnaud, H., Delanoy, G., 1995. The Lower Cretaceous
1238 Cephalopod Team First Field Meeting (Digne, 1990). The Lower Cretaceous of the South
1239 Vocontian basin and margins. Bulot et al. (eds.), Lower Cretaceous cephalopod
1240 biostratigraphy of the Western Tethys: recent developments, regional synthesis and
1241 outstanding problems. Géologie Alpine (1994), H.S. 20, 383–399.
1242 Bulot, L.G., Thieuloy, J.-P., Blanc, E., Klein, J., 1993. Le cadre stratigraphique du
1243 Valanginien supérieur et de l'Hauterivien du Sud-Est de la France : définition de
1244 biochronozones et caractérisation de nouveaux biohorizons. Géologie Alpine 68, 13–56.

1245 Bulot, L.G., Vermeulen, J., Grosheny, D., 2010. Le Crétacé de l'Arc de Castellane (SE
1246 France, 25-28 Août 2010). Excursion du Groupe Français du Crétacé, GFC 2010, Série
1247 « Excursion », 46 p. https://hal.archives-ouvertes.fr/hal-00686778
1248 Busnardo, R., Thieuloy, J.P., 1979. Les zones d'ammonites du Valanginien. In: Busnardo, R.,
1249 Thieuloy, J.P., Moullade, M. (Eds.), Hypostratotype mésogéen de l'étage Valanginien
1250 (sud-est de la France). Edition C.N.R.S (Paris), Les stratotypes français, 6, pp. 58–68.
1251 Busnardo, R., Charollais, J., Weidmann, M., Clavel, B., 2003. Le Crétacé inférieur de la
1252 Veveyse de Châtel (Ultrahelvétique des Préalpes externes ; canton de Fribourg, Suisse).
1253 Revue de Paléobiologie 22, 1–174.
1254 Canérot, J., Cugny, P., Peybernès, B., Rahli, I., Rey, J., Thieuloy, J.-P., 1986. Comparative
1255 study of the Lower and Mid-Cretaceous sequences on different maghrebian shelves and
1256 basins: Their place in the evolution of the North African, Atlantic and Neotethysian
1257 margins. Palaeogeography, Palaeoclimatology, Palaeoecology 55, 213–232.
1258 Charbonnier, G., Duchamp-Alphonse, S., Deconinck, J.-F., Adatte, T., Spangenberg, J.E.,
1259 Colin, C., Follmi, K.B., 2020. A global palaeoclimatic reconstruction for the Valanginian
1260 based on clay mineralogical and geochemical data. Earth-Science Reviews 202, 103092.
1261 Charbonnier, G., Morales, C., Duchamp-Alphonse, S., Westermann, S., Adatte, T., Follmi,
1262 K.B., 2017. Mercury enrichments indicate volcanic triggering of Valanginian
1263 environmental change. Scientific Reports 7, 40808.
1264 Coffin, M.F., Eldholm, O., 1994. Large igneous provinces: crustal structure, dimensions, and
1265 external consequences. Reviews of Geophysics 32, 1–36.
1266 Company, M., 1987. Los ammonites del Valanginiense del sector oriental de las Cordilleras
1267 Béticas (SE de España). Tesis Doctoral, Universidad de Granada, Granada, 294 pp.
1268 Company, M., Tavera, J.M., 2015. Lower Valanginian ammonite biostratigraphy in the
1269 Subbetic Domain (Betic Cordillera, southeastern Spain). Carnets de Géologie 15, 71–88.

1270 Duchamp-Alphonse, S., Gardin, S., Fiet, N., Bartolini, A., Blamart, D., Pagel, M., 2007.
1271 Fertilization of the northwestern Tethys (Vocontian basin, SE France) during the
1272 Valanginian carbon isotope perturbation: Evidence from calcareous nannofossils and trace
1273 element data. Palaeogeography, Palaeoclimatology, Palaeoecology 243, 132–151.
1274 Duffaud, F., Brun, L., Plauchut, B., 1966. Le bassin du Sud-Ouest Marocain. In: Reyre, D.
1275 (Ed.). Bassins sédimentaires du littoral Africain. Association des Services Géologiques
1276 Africains, Firmin Didot Publ. Paris, 5–12.
1277 Ellouz, N., Patriat, M., Gaulier, J.-M., Bouatmani, R., Sabounji, S., 2003. From rifting to
1278 Alpine inversion: Mesozoic and Cenozoic subsidence history of some Moroccan basins.
1279 Sedimentary Geology 156, 185–212.
1280 Erba, E., Bartolini, A., Larson, R.L., 2004. Valanginian Weissert oceanic anoxic event.
1281 Geology 32, 149–152.
1282 Ettachfini, M., 1991. Le Valanginien de l'Atlas Atlantique (Maroc): stratigraphie et
1283 ammonitofaune. Strata 2, 15, 1–177.
1284 Ettachfini, M., 2004. Les ammonites néocomiennes dans l'Atlas Atlantique (Maroc) :
1285 biostratigraphie, paléontologie, paléobiogéographie et paléoécologie. Strata 2, 43, 225 pp.
1286 Fanti, F., Contessi, M., Franchi, F., 2012. The "Continental Intercalaire" of southern Tunisia:
1287 Stratigraphy, paleontology, and paleoecology. Journal of African Earth Sciences 73-74, 1–
1288 23.
1289 Ferry, S., Masrour, M., Grosheny, D., 2007. Le Crétacé de la marge atlantique marocaine
1290 (région d'Agadir). Excursion du Groupe Français du Crétacé, Livret-guide, 70 pp.
1291 https://hal.archives-ouvertes.fr/hal-00686791/fr/
1292 Föllmi, K., 2012. Early Cretaceous life, climate and anoxia. Cretaceous Research 35, 230–
1293 357.

1294 Föllmi, K.B., Weissert, H., Bisping, M., Funk, H., 1994. Phosphogenesis, carbon–isotope
1295 stratigraphy, and carbonate–platform evolution along the Lower Cretaceous northern
1296 Tethyan margin. Geological Society of America Bulletin 106, 729–746.
1297 Frizon de Lamotte, D., Leturmy, P., Missenard, Y., Khomsi, S., Ruiz, G., Saddiqi, O.,
1298 Guillocheau, F., Michard, A., 2009. Mesozoic and Cenozoic vertical movements in the
1299 Atlas system (Algeria, Morocco, Tunisia): An overview. Tectonophysics 475, 9–28.
1300 Frizon de Lamotte, D., Saint Bezar, B., Bracène, R., 2000. The two main steps of the Atlas
1301 building and geodynamics of the western Mediterranean. Tectonics 19, 740–761.
1302 Gale, A.S., 2020. Roveacrinidae (Crinoidea, Articulata) from the Cenomanian and Turonian
1303 of North Africa (Agadir Basin and Anti-Atlas, Morocco, and central Tunisia):
1304 biostratigraphy and taxonomy. Acta Geologica Polonica 70, 273−310.
1305 Gale, A.S., Mutterlose, J., Batenburg., S., Gradstein, F.M., with the contribution of Agterberg,
1306 F.P., Ogg, J.G., Petrizzo, M.R., 2020. The Cretaceous Period. In: Gradstein et al. (eds),
1307 Geologic Time Scale 2020, 1023-1086.
1308 Gauthier, H. (Ed.), Busnardo, R., Combémorel, R., Delanoy, G., Fischer, J.-C., Guérin-
1309 Franiatte, S., Joly, B., Kennedy, W.J., Sornay, J., Tintant, H., 2006. Révision critique de la
1310 Paléontologie française d'Alcide d'Orbigny. Volume IV. Céphalopodes crétacés. Backhuys
1311 Publisher, Leiden, 292 pp.
1312 Godet, A., Durlet, C., Spangenberg, J.E., Föllmi, K.B., 2016. Estimating the impact of early
1313 diagenesis on isotope records in shallow-marine carbonates: A case study from the
1314 Urgonian Platform in western Swiss Jura. Palaeogeography, Palaeoclimatology,
1315 Palaeoecology 454, 125–138.
1316 Gollain, B., Mattioli, E., Kenjo, S., Bartolini, A., Reboulet, S., 2019. Size-patterns of the
1317 coccolith *Watznaueria barnesiae* in the Lower Creataceous: biotic *versus* abiotic forcing.
1318 Marine Micropaleontology 152, 101740.

1319 Gomes, A.S., Vasconcelos, P.M., 2021. Geochronology of the Paraná-Etendeka large igneous
1320 province. Earth-Science Reviews 220, 103716.
1321 Gradinaru, M., Lazar, J., Bucur, I.I., Gradinaru, E., Sasaran, E., Ducea, M.N., Andrasanu, A.,
1322 2016. The Valanginian history of the eastern part of the Getic Carbonate Platform
1323 (Southern Carpathians, Romania): Evidence for emergence and drowning of the platform.
1324 Cretaceous Research 66, 11–42.
1325 Gréselle, B., Pittet, B., 2010. Sea-level reconstructions from the Peri-Vocontian Zone (South-
1326 east France) point to Valanginian glacio-eustasy. Sedimentology 57, 1640–1684.
1327 Gréselle, B., Pittet, B., Mattioli, E., Joachimski, M., Barbarin, N., Riquier, L., Reboulet, S.,
1328 Pucéat, E., 2011. The Valanginian isotope event: A complex suite of palaeoenvironmental
1329 perturbations. Palaeogeography Palaeoclimatology Palaeoecology 306, 41–57.
1330 Gröcke, D.R., Price, G.D., Robinson, S.A., Baraboshkin, E.Y., Mutterlose, J., Ruffell, A.H.,
1331 2005. The Upper Valanginian (Early Cretaceous) positive carbon-isotope event recorded in
1332 terrestrial plants. Earth and Planetary Science Letters 240, 495–509.
1333 Guiraud, R., Bosworth, W., 1997. Senonian inversion and rejuvenation of rifting in Africa and
1334 Arabia: synthesis and implications to plate-scale tectonics. Tectonophysics 282, 39–82.
1335 Hafid, M., Tari, G., Bouhadioui, D., El Moussaid, I., Aït Salem, A., Nahim, M., Dakki, M.,
1336 2008. Atlantic Basins. In: Michard, A. et al. (Eds), Continental Evolution: the Geology of
1337 Morocco. Lecture Notes in Earth Sciences 116, 303–329.
1338 Haq, B.U., 2014. Cretaceous eustasy revisited. Global and Planetary Change 113, 44–58.
1339 Hedberg, H.D., 1976. International stratigraphic guide. A Guide to Stratigraphic
1340 Classification, Terminology, and Procedure. Wiley J. and Sons, New York, 200 pp.
1341 Hennig, S., Weissert, H., Bulot, L., 1999. C-isotope stratigraphy, a calibration tool between
1342 ammonite- and magnetostratigraphy: the Valanginian–Hauterivian transition. Geologica
1343 Carpathica 50, 91–96.

Hoedemaeker, P.J., Reboulet, S., (reporters), Aguirre-Urreta, M.B., Alsen, P., Aoutem, M., Atrops, F., Barragán, R., Company, M., González-Arreola, C., Klein, J., Lukeneder, A., Ploch, I., Raisossadat, N., Rawson, P.F., Ropolo, P., Vašíček, Z., Vermeulen, J., Wippich M.G.E., 2003. Report on the 1st International Workshop of the IUGS Lower Cretaceous Ammonite Working Group, the "Kilian Group" (Lyon, 11 July 2002). Cretaceous Research 24, 89–94, and erratum (p. 805).

Jaillard, E., Al Yacoubi, L., Reboulet, S., Robert, E., Masrour, M., Bouchaou, L., Giraud, F., El Hariri, K., 2019a. Late Barremian eustacy and tectonism in the western High Atlas (Essaouira-Agadir Basin), Morocco. Cretaceous Research 93, 225–244.

Jaillard, E., Hassanein Kassab, W., Giraud, F., Robert, E., Masrour, M., El Hariri, K., Mohamed F. Aly, M.F., 2019b. Aptian-lower Albian sedimentation in the Essouira-Agadir basin, western Morocco, Cretaceous Research 102, 59–80.

Joly, B., 2000. Les Juraphyllitidae, Phylloceratidae, Neophylloceratidac (Phylloceratacеae, Phylloceratina, Ammonoidea) de France au Jurassique et au Crétacé. Geobios, Mémoire Spécial 23, and Mémoire de la Société Géologique de France 174, 204 pp.

Kender, S., Kaminski, M.A., 2017. Modern deep-water agglutinated foraminifera from IODP Expedition 323, Bering Sea: ecological and taxonomic implications. Journal of Micropalaeontology 36, 195–218.

Kenjo, S., 2014. Biostratigraphie intégrée à nannofossiles calcaires et ammonoïdes : développement et implications pour la définition et la valorisation des stratotypes d'unité et de limite. L'exemple des étages Berriasien et Valanginien et de leur limite (140 Millions d'années). Unpublished PhD thesis, Université de Lyon, 226 pp.

Kenjo, S., Reboulet S., Mattioli, E., Ma'louleh, K., 2021. The Berriasian–Valanginian boundary in the Mediterranean Province of the Tethyan Realm: Ammonite and calcareous

1368 nannofossil biostratigraphy of the Vergol section (Montbrun-les-Bains, SE France),
1369 candidate for the Valanginian GSSP. Cretaceous Research 121, 104738.
1370 Kessels, K., Mutterlose, J., Michalzik, D., 2006. Early Cretaceous (Valanginian - Hauterivian)
1371 calcareous nannofossils and isotopes of the northern hemisphere: Proxies for the
1372 understanding of Cretaceous climate. Lethaia 39, 157–172.
1373 Klein, J., 2005. Lower Cretaceous Ammonites I, Perisphinctaceae 1: Himalayitidae,
1374 Olcostephanidae, Holcodiscidae, Neocomitidae, Oosterellidae. In: Riegraf, W. (Ed.),
1375 Fossilium Catalogus I: Animalia. Backhuys Publishers, Leiden, Netherlands, Pars 139, 484
1376 pp.
1377 Klein, J., Busnardo, R., Company, M., Delanoy, G., Kakabadze, M., Reboulet, S., Ropolo, P.,
1378 Vašíček, Z., Vermeulen, J., 2007. Lower Cretaceous Ammonites III. Bochianitoidea,
1379 Protancyloceratoidea, Ancyloceratoidea, Ptychoceratoidea. In: Riegraf, W. (Ed.),
1380 Fossilium Catalogus I: Animalia. Backhuys Publishers, Leiden, Netherlands, Pars 144, 381
1381 pp.
1382 Klein, J., Hoffmann, R., Joly, B., Shigeta, Y., Vašíček, Z., 2009. Lower Cretaceous
1383 Ammonites IV. Boreophylloceratoidea, Phylloceratoidea, Lytoceratoidea, Tetragonitoidea,
1384 Haploceratoidea including the Upper Cretaceous representatives. In: Riegraf, W. (Ed.),
1385 Fossilium Catalogus I: Animalia. Backhuys Publishers, Leiden, Netherlands, Pars 146, 416
1386 pp.
1387 Kuhnt, W., Moullade, M., Kaminski, M.A., 1996. Ecological structuring and evolution of
1388 deep-sea agglutinated foraminifera - A review. Revue de Micropaléontologie 39, 271–281.
1389 Kujau, A., Heimhofer, U., Ostertag-Henning, C., Gréselle, B., Mutterlose, J., 2012. No
1390 evidence for anoxia during the Valanginian carbon isotope event – An organic-
1391 geochemical study from the Vocontian Basin, SE France. Global and Planetary Change
1392 92–93, 92–104.

1393 Lefranc, J.-P., Guiraud, R., 1990. Continental Intercalaire of northwestern Sahara and its
1394 equivalents in the neighbouring regions. Journal of African Earth Sciences 10, 27-77.
1395 Le Hégarat, G., 1973. Le Berriasien du Sud-Est de la France. Documents des Laboratoires de
1396 Géologie, Faculté des Sciences de Lyon 43 (1971), 576 pp.
1397 Le Roy, P., Guillocheau, F., Piqué, A., Morabet, A.M., 1998. Subsidence of the Atlantic
1398 Moroccan margin during the Mesozoic. Canadian Journal of Earth Sciences 35, 476–493.
1399 Lini, A., Weissert, H., Erba, E., 1992. The Valanginian carbon isotope event: a first episode of
1400 greenhouse climate conditions during the Cretaceous. Terra Nova 4, 374–384.
1401 Luber, T.L., Bulot, L.G., Redfern, J., Frau, C., Arantegui, A., Masrour, M., 2017. A revised
1402 ammonoid biostratigraphy for the Aptian of NW Africa: Essaouira-Agadir Basin.
1403 Cretaceous Research 79, 12–34.
1404 Martinez, M., Deconinck, J.-F., Pellenard, P., Reboulet, S., Riquier, L., 2013.
1405 Astrochronology of the Valanginian stage from reference sections (Vocontian Basin,
1406 France) and palaeoenvironmental implications for the Weissert Event. Palaeogeography,
1407 Palaeoclimatology, Palaeoecology 376, 91–102.
1408 Martinez, M., Deconinck, J-F., Pellenard, P., Riquier, L., Company, M., Reboulet, S.,
1409 Moiroud, M., 2015. Astrochronology of the Valanginian–Hauterivian stages (Early
1410 Cretaceous): chronological relationships between the Paraná–Etendeka large igneous
1411 province and the Weissert and the Faraoni events. Global and Planetary Change 131, 158–
1412 173.
1413 Masse, J.-P., Lesbros, R., 1987. Evénements géodynamiques médio-valanginiens dans le S-E
1414 de la France et leur retentissements bathymétriques. Leur signification dans le cadre
1415 géodynamique de la Méditerranée occidentale. Mémoire géologique de l'université de
1416 Dijon 11, 149–156.

McArthur, J.M., Janssen, N.M.M., Reboulet, S., Leng, M.J., Thirlwall, M.F., van de Schootbrugge, B., 2007. Palaeotemperatures, polar ice-volume, and isotope stratigraphy (Mg/Ca, $\delta^{18}O$, $\delta^{13}C$, $^{87}Sr/^{86}Sr$): The Early Cretaceous (Berriasian, Valanginian, Hauterivian). Palaeogeography, Palaeoclimatology, Palaeoecology 248, 391–430.

Melinte, M., Mutterlose, J., 2001. A Valanginian (Early Cretaceous) "boreal nannoplankton excursion" in sections from Romania. Marine Micropaleontology 43, 1–25.

Melliti, S., Reboulet, S., Ben Haj Ali, N., Arfaoui, M.S., Zargouni, F., Memmi, L., 2019. Ammonoid and foraminiferal biostratigraphy from uppermost Valanginian to lowermost Barremian of the Jebel Boulahouajeb section (northern Tunisia). Journal of African Earth Sciences 151, 438–460.

Möller, C., Mutterlose, J., Alsen, P., 2015. Integrated stratigraphy of Lower Cretaceous sediments (Ryazanian–Hauterivian) from North-East Greenland. Palaeogeography, Palaeoclimatology, Palaeoecology 437, 85–97.

Morales, C., Gardin, S., Schnyder, J., Spangenberg, J., Arnaud-Vanneau, A., Arnaud, H., Adatte, T., Föllmi, K.B., 2013. Berriasian and early Valanginian environmental change along a transect from the Jura Platform to the Vocontian Basin. Sedimentology 60, 36–63.

Mourgues, F.A., Bulot, L.G., Frau, C., 2015. The Valanginian Olcostephaninae Haug, 1910 (Ammonoidea) from the Andean Lower Cretaceous Chañarcillo Basin, Northern Chile. Andean Geology 42, 213–236.

Mutterlose, J., Rawson, P.F., Reboulet, S., with contributions by Baudin, F., Bulot, L., Emmanuel, L., Gardin, S., Martinez, M., Renard, M., 2020. The Global Boundary Stratotype Section and Point (GSSP) for the base of the Hauterivian Stage (Lower Cretaceous), La Charce, southeast France. Episodes, Communication of IUGS Geological Standards, 1–22.

1441 Newell, A.J., Kirby, G.A., Sorensen, J.P.R., Milodowski, A.E., 2015. The Cretaceous
1442 Continental Intercalaire in central Algeria: Subsurface evidence for a fluvial to aeolian
1443 transition and implications for the onset of aridity on the Saharan Platform.
1444 Palaeogeography, Palaeoclimatology, Palaeoecology 438, 146–159.
1445 Perch-Nielsen, K., 1979. Calcareous nannofossils from the Cretaceous between the North Sea
1446 and the Mediterranean. Aspekte der Kreide Europas. IUGS Series A 6, 223–272.
1447 Perch-Nielsen, K., 1985. Mesozoic Calcareous nannofossils. In: Bolli, H. M., Saunders, J. B.,
1448 Perch-Nielsen K. (Eds), Plankton stratigraphy, Cambridge University Press, Cambridge,
1449 329–426.
1450 Price, G.D., 1999. The evidence and implications of polar ice during the Mesozoic. Earth-
1451 Science Reviews 48, 183–210.
1452 Pucéat, E., Lecuyer, C., Sheppard, S.M.F., Dromart, G., Reboulet, S., Grandjean, P., 2003.
1453 Thermal evolution of Cretaceous Tethyan marine waters inferred from oxygen isotope
1454 composition of fish tooth enamels. Paleoceanography, 18, 2, 1029.
1455 Rawson, P.F., 2007. Global relationships of Argentine (Neuquén Basin) Early Cretaceous
1456 ammonite faunas. Geological Journal 42, 175–183.
1457 Reboulet, S., 1996. L'évolution des ammonites du Valanginien-Hauterivien inférieur du
1458 bassin vocontien et de la plate-forme provençale (S-E de la France) : relations avec la
1459 stratigraphie séquentielle et implications biostratigraphiques. Documents des Laboratoires
1460 de Géologie Lyon 137 (1995), 371 pp.
1461 Reboulet, S., 2008. Origination of *Himantoceras* (heteromorphic ammonoids) related to
1462 palaeoceanography and climatic changes during the Valanginian. 1st International Meeting
1463 on Correlation of Cretaceous Micro- and Macrofossils, Vienna (Austria), 16–18 April,
1464 2008, Berichte der Geologischen Bundesanstalt 74, 89–91.

Reboulet, S., Atrops, F., 1999. Comments and proposals about the Valanginian–lower Hauterivian ammonite zonation of south-eastern France. Eclogae Geologicae Helvetiae 92, 183–197.

Reboulet, S., Atrops, F., Ferry, S., Schaaf, A., 1992. Renouvellement des ammonites en fosse vocontienne à la limite Valanginien–Hauterivien. Géobios 25, 469–476.

Reboulet, S., Hoedemaeker, P.J., (reporters), Aguirre-Urreta, M.B., Alsen, P., Atrops, F., Baraboshkin, E.Y., Company, M., Delanoy, G., Dutour, Y., Klein, J., Latil, J.L., Lukeneder, A., Mitta, V., Mourgues, F.A., Ploch, I., Raisossadat, N., Ropolo, P., Sandoval, J., Tavera, J.M., Vašíček, Z., Vermeulen, J., 2006. Report on the 2nd international meeting of the IUGS Lower Cretaceous ammonite working group, the "Kilian Group" (Neuchâtel, Switzerland, 8 September 2005). Cretaceous Research 27, 712–715.

Reboulet, S., Klein, J. (reporters), Barragán, R., Company, M., González-Arreola, C., Lukeneder, A., Raisossadat, S.N., Sandoval, J., Szives, O., Tavera, J.M., Vašíček, Z., Vermeulen, J., 2009. Report on the 3rd International Meeting of the IUGS Lower Cretaceous AmmoniteWorking Group, the "Kilian Group" (Vienna, Austria, 15th April 2008). Cretaceous Research 30, 496–502.

Reboulet, S., Mattioli, E., Pittet, B., Baudin, F., Olivero, D., Proux, O., 2003. Ammonoid and nannoplankton abundance in Valanginian (early Cretaceous) limestone-marl successions from the southeast France Basin: carbonate dilution or productivity? Palaeogeography, Palaeoclimatology, Palaeoecology 201, 113–139.

Reboulet, S., Rawson, P.F., Moreno-Bedmar, J.A. (reporters), Aguirre-Urreta, M.B., Barragán, R., Bogomolov, Y., Company, M., González-Arreola, C., Idakieva Stoyanova, V., Lukeneder, A., Matrion, B., Mitta, V., Randrianaly, H., Vašíček, Z., Baraboshkin, E.J., Bert, D., Bersac, S., Bogdanova, T.N., Bulot, L.G., Latil, J.-L., Mikhailova, I.A., Ropolo, P., Szives, O., 2011. Report on the 4th International Meeting of the IUGS Lower

1490 Cretaceous Ammonite Working Group, the “Kilian Group” (Dijon, France, 30th August
1491 2010). Cretaceous Research 32, 786–793.
1492 Reboulet, S., Szives, O. (reporters), Aguirre-Urreta, B., Barragán, R., Company, M., Frau, C.,
1493 Kakabadze, M.V., Klein, J., Moreno-Bedmar, J.A., Lukeneder, A., Pictet, P., Ploch, I.,
1494 Raisossadat, S.N., Vašíček, Z., Baraboshkin, E.J., Mitta, V.V., 2018. Report on the 6th
1495 International Meeting of the IUGS Lower Cretaceous Ammonite Working Group, the
1496 Kilian Group (Vienna, Austria, 20th August 2017). Cretaceous Research 91, 100–110.
1497 Reboulet, S., Szives, O. (reporters), Aguirre-Urreta, B., Barragán, R., Company, M., Idakieva,
1498 V., Ivanov, M., Kakabadze, M.V., Moreno-Bedmar, J.A., Sandoval, J., Baraboshkin, E.J.,
1499 Çağlar, M.K., Főzy, I., González-Arreola, C., Kenjo, S., Lukeneder, A., Raisossadat, S.N.,
1500 Rawson, P.F., Tavera, J.M., 2014. Report of the 5th International Meeting of the IUGS
1501 Lower Cretaceous Ammonite Working Group, the Kilian Group (Ankara, Turkey, 31st
1502 August 2013). Cretaceous Research 50, 126–137.
1503 Rey, J., Canérot, J., Peybernès, B., Taj-Eddine, K., Rahhali, I., Thieuloy, J-P. 1986. Le
1504 Crétacé inférieur de la région d’Essaouira : données biostratigraphiques et évolutions
1505 sédimentaires. PICG – UNESCO section Sciences de la Terre 183, Revue de la Faculté des
1506 sciences de Marrakech, numéro spécial 2, 413–441.
1507 Rey, J., Canérot, J., Peybernès, B., Taj-Eddine, K., Thieuloy, J.-P., 1988. Lithostratigraphy,
1508 biostratigraphy and sedimentary dynamics of the Lower Cretaceous deposits on the
1509 northern side of the western High Atlas (Morocco). Cretaceous Research 9, 141–158.
1510 Roch, E., 1930. Une histoire stratigraphique du Maroc. Notes et Mémoires du Service
1511 géologique du Maroc 80, 440 pp.
1512 Roth, P.H., 1978. Cretaceous Nannoplankton Biostratigraphy and Oceanography of the
1513 Northwestern Atlantic Ocean. In: Benson, W. E., Sheridan, R. E., Pastouret, L., Enos, P.,

Freeman, T., Murdmaa, I. O., Worstell, P. (editor), Gradstein, F., Schmidt, R. R., Weaver, F. M., Stuermer, D. H., Initial reports of the Deep Sea Drilling Project 44, 731–759.

Schlager, W., 1980. Mesozoic calciturbidites in Deep Sea Drilling Project Hole 416A: Recognition of a drowned carbonate platform. In: Lancelot, Y., Winterer, E.L. (eds): Initial Reports of the Deep Sea Drilling Project, 50, Washington D.C., U.S. Gov. Print. Off., 733–749.

Schwarz, E., Buatois, L.A., 2012. Substrate-controlled ichnofacies along a marine sequence boundary: The Intra-Valanginian Discontinuity in central Neuquén Basin (Argentina). Sedimentary Geology 277–278, 72–87.

Shmeit, M., Giraud, F., Jaillard, E., Reboulet, S., Masrour, M., Spangenberg, J.E., El-Samrani, A., 2022. The Valanginian Weissert Event on the south Tethyan margin: A dynamic paleoceanographic evolution based on the study of calcareous nannofossils. Marine Micropaleontology 175, 102134.

Sissingh, W., 1977. Biostratigraphy of Cretaceous Calcareous Nannoplankton. Geology en Mijnbouw 56, 37–65.

Soua, M., 2016. Cretaceous oceanic anoxic events (OAEs) recorded in the northern margin of Africa as possible oil and gas shale potential in Tunisia: An overview. International Geology Review 58, 277-320.

Sprovieri, M., Coccioni, R., Lirer, F., Pelosi, N., Lozar, F., 2006. Orbital tuning of a lower Cretaceous composite record (Maiolica Formation, central Italy). Paleoceanography 21, PA4212.

Taj-Eddine, K., Ettachfini, El M., Rey J., 1992. Le Berriasien et le Valanginien de l'Atlas Atlantique - Maroc. Biostratigraphie et séquences de dépôt. Géologie Méditerranéenne 19, 41–50.

1538 Thieuloy, J.P., 1977. La zone à Callidiscus du Valanginien supérieur vocontien (Sud-Est de la
1539 France). Lithostratigraphie, ammonitofaune, limite Valanginien–Hauterivien, corrélations.
1540 Géologie Alpine 53, 83–143.
1541 Thieuloy, J.P., Bulot, L., 1992. Ammonites du Crétacé inférieur du Sud-Est de la France : 1.
1542 Nouvelles espèces à valeur stratigraphique pour le Valanginien et l'Hauterivien. Géologie
1543 Alpine 68, 85–103.
1544 Thieuloy, J.-P., Fuhr, M., Bulot, L., 1990. Biostratigraphie du Crétacé inférieur de l'Arc de
1545 Castellane (S.E. de la France). 1 : Faunes d'ammonites du Valanginien supérieur et âge de
1546 l'horizon dit de "La Grande Lumachelle". Géologie Méditerranéenne 17, 55–99.
1547 Vašíček, Z., 2020. *Teschениceras* gen. nov. (Ammonoidea) and the definition of the
1548 Valanginian/Hauterivian boundary in Butkov Quarry (Central Western Carpathians,
1549 Slovakia). Acta Geologica Polonica 70, 569–584.
1550 Wiedmann, J., Butt, A., Einsele, G., 1982. Cretaceous Stratigraphy, Environment, and
1551 Subsidence History at the Moroccan Continental Margin. In: von Rad, U. et al. (Eds.),
1552 Geology of the Northwest African Continental Margin, 366–395, Springer-Verlag.
1553 Wippich, M.G.E., 2001. Die tiefe Unter-Kreide (Berrias bis Unter-Hauterive) im
1554 südwestmarokkanischen Becken: Ammonitenfauna, Bio-und Sequenzstratigraphie.
1555 Unpublished PhD thesis, Universität Bochum, 142 pp.
1556 Wippich, M.G.E., 2003. Valanginian (Early Cretaceous) ammonite faunas from the western
1557 High Atlas, Morocco, and the recognition of western Mediterranean "standard" zones.
1558 Cretaceous Research 24, 357–374.
1559 Witam, O., 1998. Le Barrémien-Aptien de l'Atlas Occidental (Maroc) : lithostratigraphie,
1560 biostratigraphie, sédimentologie, stratigraphie séquentielle, géodynamique et
1561 paléontologie. Strata 30, 1–421.

Zühlke, R., Bouaouda, M.-S., Ouajhain, B., Bechstädt, T., Leinfelder, R., 2004. Quantitative Meso/Cenozoic development of the eastern Central Atlantic continental Shelf, western High Atlas, Morocco. Marine and Petroleum Geology 21, 225–276.

Figure captions

Figure 1. Location of the study area. A. Location of the Essaouira-Agadir Basin (EAB). B. Geological sketch of the EAB, and location of the studied sections (black squares). The east–west transect of sections illustrated in Fig. 2 is represented by a black line.

Figure 2. The Berriasian–lower Hauterivian sedimentary evolution in the southern part of the Essaouira-Agadir Basin. Simplified from Ferry et al. (2007). Note the eastward retrogradation of facies during the Berriasian–upper Valanginian interval, and the westward progradation in the lower Hauterivian. Among the successions illustrated here, only Aït Hamouch was selected for the present work.

Figure 3. The Zalidou section. Stratigraphic distribution of macrofauna (mainly ammonites; a question mark is added when identification is doubtful) and ammonite zonation (standard and local units); layers of sampling are indicated at the right of the succession. Nannofossil zonation (NK, NC and CC) and bioevents (FO and LO) from Shmeit et al. (2022) and completed in this work. The NK and NC zones are from Bralower (1987), Bralower et al. (1989; 1995), modified from Roth (1978). The CC zones and subzones are from Sissingh (1977), modified by Perch-Nielsen (1979; 1985) and Applegate and Bergen (1988).

Sedimentary discontinuities (D). Carbon isotopic curve; layers of sampling are indicated at the left of the succession. The lower–upper Valanginian boundary is preferentially placed at the base of layers ZA40 (boundary indicated by a solid line); an alternative proposal (ZA36, boundary indicated by a dashed line) is discussed in the text (see 4.1. Ammonite stratigraphy).

Figure 4. The Aït Hamouch section (two outcrops). Stratigraphic distribution of macrofauna (mainly ammonites; a question mark is added when identification is doubtful) and ammonite zonation (standard and local units); layers of sampling are indicated at the right of the succession. Nannofossil zonation (NK, NC and CC) and bioevents (FO and LO) from Shmeit et al. (2022) and completed in this work. Sedimentary discontinuities (D). Carbon isotopic curve; layers of sampling are indicated at the left of the succession. The alphanumeric notation is "AH", except for the interval between 32 and 50.5 m of the right-hand column where "AtH" is used (AtH1 to AtH18).

Figure 5. The Zaouia Sidi Abderahmane section (two outcrops). Stratigraphic distribution of macrofauna (mainly ammonites; a question mark is added when identification is doubtful) and ammonite zonation (standard and local units); layers of sampling are indicated at the right of the succession. Sedimentary discontinuities (D). Carbon isotopic curve; layers of sampling are indicated at the left of the succession.

Figure 6. The Igouzoulen section. Stratigraphic distribution of macrofauna (mainly ammonites; a question mark is added when identification is doubtful) and ammonite zonation (standard and local units); layers of sampling are indicated at the right of the succession. Sedimentary discontinuities (D). Carbon isotopic curve; layers of sampling are indicated at

1609 the left of the succession. The alphanumeric notation is “IGz”, except in the basal part of the
1610 section (between 12 and 16.3 m) where “IGb” is used.
1611
1612 Figure 7. The Ida w Iddar section. Stratigraphic distribution of macrofauna (mainly
1613 ammonites; a question mark is added when identification is doubtful) and ammonite zonation
1614 (standard and local units); layers of sampling are indicated at the right of the succession.
1615 Sedimentary discontinuities (D). Carbon isotopic curve; layers of sampling are indicated at
1616 the left of the succession.
1617
1618 Figure 8. The Obbay section. Stratigraphic distribution of macrofauna (mainly ammonites; a
1619 question mark is added when identification is doubtful) and ammonite zonation (standard and
1620 local units); layers of sampling are indicated at the right of the succession. Sedimentary
1621 discontinuities (D).
1622
1623 Figure 9. Calcareous nannofossil events and zonation calibrated with the ammonite standard
1624 zonation of the Essaouira-Agadir Basin (this study) and their comparisons with existing
1625 Tethyan biozonal schemes where both ammonite and nannofossil records are also available:
1626 South–east France modified from Bergen (1994); Vergol-La Charce composite section
1627 (Vocontian Basin) modified after Gréselle et al. (2011), Mutterlose et al. (2020) and Kenjo et
1628 al. (2021); Angles section (Vocontian Basin) modified after Duchamp-Alphonse et al. (2007);
1629 Cehingin area (Subbetic Basin, SE Spain) modified after Aguado et al. (2000; 2018). The FO
1630 of *E. striatus* is situated in the *K. inostranzewi* StZ or *S. verrucosum* StZ according to the
1631 ammonite biostratigraphic interpretation of the Zalidou section (see 4.1. Ammonite
1632 stratigraphy).
1633

Figure 10. Sedimentology, sequence stratigraphy and correlations (south–north transect) of Aït Hamouch, Zaouia Sidi Abderahmane and Zalidou sections from the southern part of the studied area. Caption on Fig. 11. Location on Fig. 1B.

Figure 11. Sedimentology, sequence stratigraphy and correlations (west–east transect) of Obbay, Igouzoulen and Ida w Iddar sections from the northern part of the studied area. Location on Fig. 1B.

Figure 12. Discontinuities and depositional sequences along a SSW–NNE transect including the Aït Hamouch, Zalidou and Ida w Iddar sections.

Figure 13. Correlations of the Essaouira-Agadir Basin (South Tethyan margin) with the south–east France Basin (North Tethyan margin). Lithological successions and carbon isotopic curves are simplified: Zalidou and Aït Hamouch sections after this work (Figs. 3 and 4, respectively); Vergol-La charce composite section (Vocontian Basin) modified after Reboulet (1996), Gollain et al. (2019) and Kenjo et al. (2021), and completed for the lower Valanginian *p.p* by the isotopic data (dashed line) from the Angles section (Duchamp-Alphonse et al., 2007); Carajuan section (Provence Platform) modified after Bulot (1995), Reboulet (1996), Reboulet et al. (2003) and Gréselle and Pittet (2010). Note that the thickness scale of south–east France sections is 25% that of the Moroccan sections. For the Vocontian basinal section, the calcareous bundles are indicated and named according to the ammonite zonation; “Barrande” correspond to four organic-matter-rich layers (Reboulet et al., 2003); the shaded area is the interval of the Weissert Event from the onset of the carbon isotope excursion (CIE, indicated by a black arrow) until its climax (according to Erba et al., 2004). For the Carajuan section, F1 to F13 correspond to some sedimentary formations (see

1659 references above); the zonal scheme was updated according to the standard zonation
1660 (Reboulet et al., 2018). D1 to D8: Moroccan discontinuities after this work (Figs. 3–4); DCB:
1661 “Discontinuité au toit des Calcaires Blancs” after Bulot et al. (1995; 1997); SB D to SB H:
1662 discontinuities of Gréselle and Pittet (2010); DVM and DVS: “discontinuité du Valanginien
1663 moyen” and “discontinuité du Valanginien supérieur” of Autran (1993), respectively; DVT:
1664 “discontinuité du Valanginien terminal” of Bulot et al. (2010).

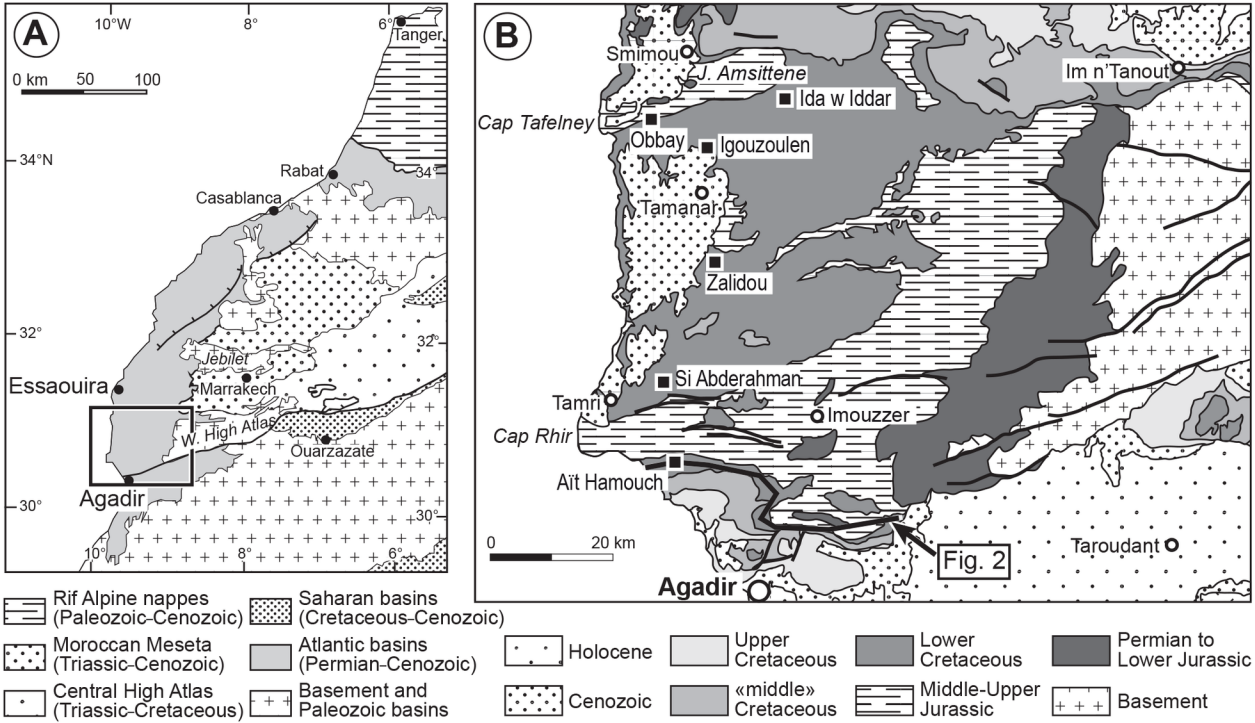
A
10°W
8°
6°
Tanger
0 km 50 100
34°N
Rabat
34°
Casablanca
32°
32°
Jebilet
Essaouira
Marrakech
W. High Atlas
Ouarzazate
Agadir
30°
30°
10°
8°
6°
B
Smimou
J. Amsittene
Ida w Iddar
Im n'Tanout
Cap Tafelney
Obbay
Igouzoulen
Tamanar
Zalidou
Si Abderahman
Tamri
Imouzzer
Cap Rhir
Aït Hamouch
0 20 km
Fig. 2
Taroudant
Agadir
Rif Alpine nappes (Paleozoic-Cenozoic)
Saharan basins (Cretaceous-Cenozoic)
Moroccan Meseta (Triassic-Cenozoic)
Atlantic basins (Permian-Cenozoic)
Central High Atlas (Triassic-Cretaceous)
Basement and Paleozoic basins
Holocene
Upper Cretaceous
Lower Cretaceous
Permian to Lower Jurassic
Cenozoic
«middle» Cretaceous
Middle-Upper Jurassic
Basement

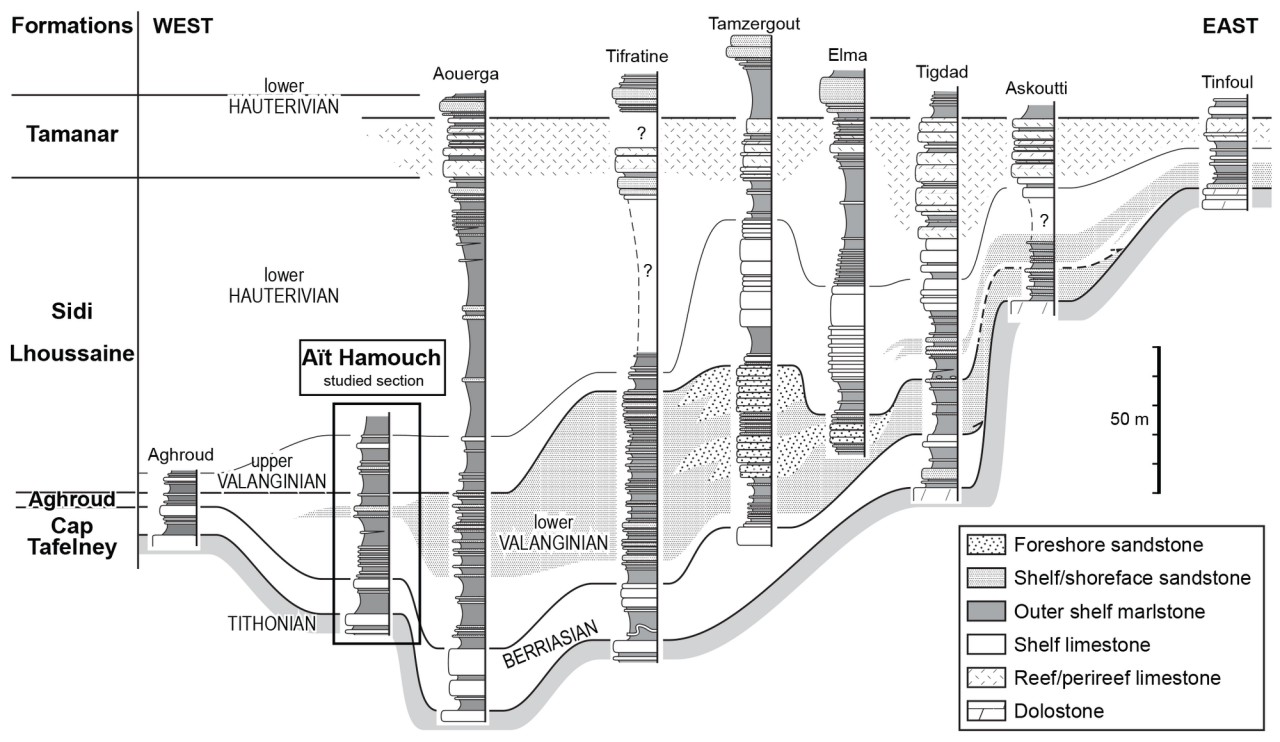
Formations
WEST
EAST
Tamzergout
Tifratine
Aouerga
Elma
Tigdad
Askoutti
Tinfoul
lower
HAUTERIVIAN
Tamanar
?
?
?
lower
HAUTERIVIAN
Sidi
Lhoussaine
Aït Hamouch
studied section
50 m
Aghroud
upper
VALANGINIAN
Aghroud
Cap
Tafelney
lower
VALANGINIAN
TITHONIAN
BERRIASIAN
Foreshore sandstone
Shelf/shoreface sandstone
Outer shelf marlstone
Shelf limestone
Reef/perireef limestone
Dolostone

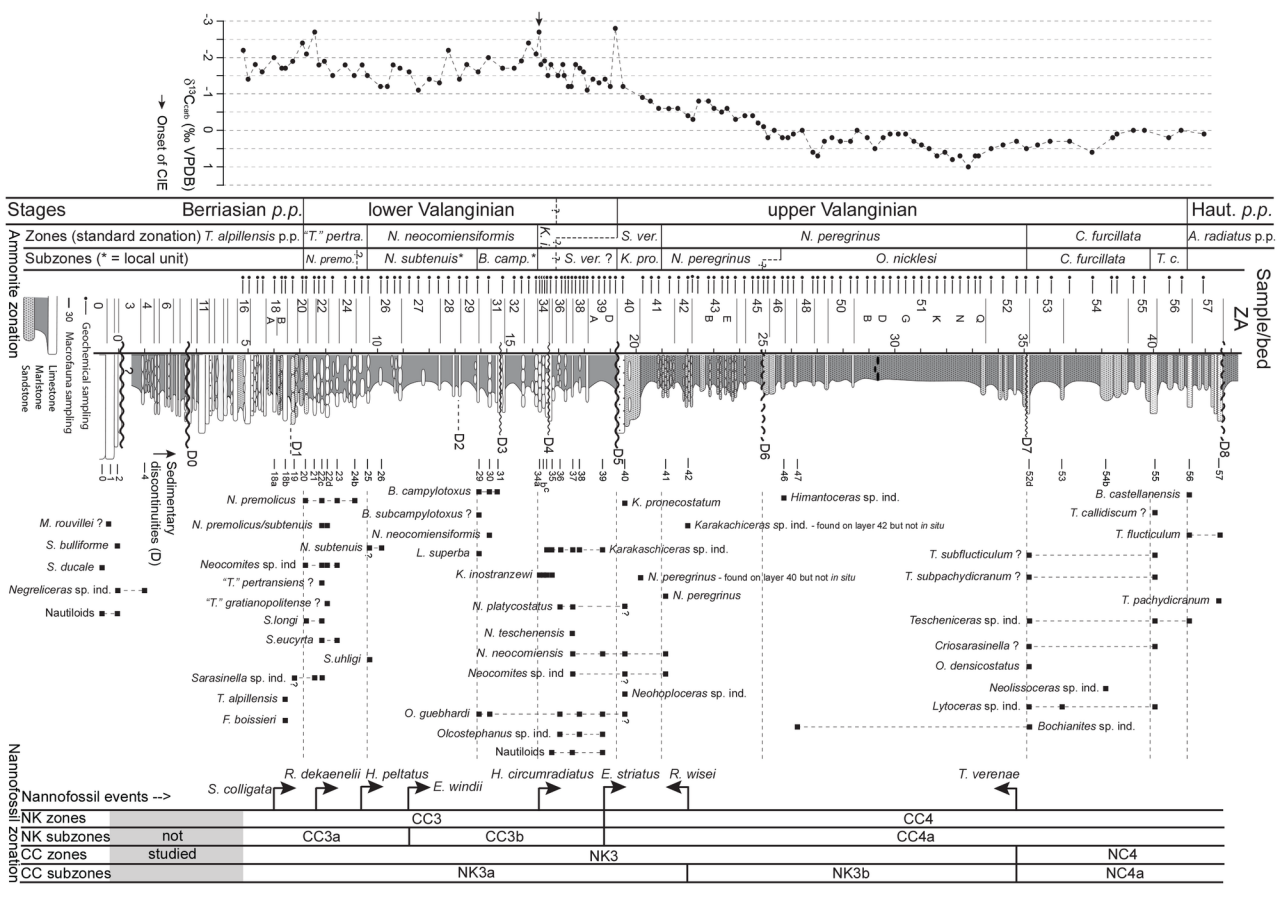
δ13Ccarb (‰ VPDB)
→ Onset of CIE
Stages
Berriasian p.p.
lower Valanginian
upper Valanginian
Haut. p.p.
Zones (standard zonation) T. alpillensis p.p.
"T." pertra.
N. neocomiensiformis
K. l.
S. ver.
N. peregrinus
C. furcillata
A. radiatus p.p.
Subzones (* = local unit)
N. premo.
N. subtenuis*
B. camp.*
-? S. ver. ?
K. pro.
N. peregrinus
O. nicklesi
C. furcillata
T. c.
Ammonite zonation
Sample/bed
ZA
Geochemical sampling
Macrofauna sampling
Limestone
Marlstone
Sandstone
Sedimentary discontinuities (D)
D0
D1
D2
D3
D4
D5
D6
D7
D8
N. premolicus
M. rouvillei ?
S. bulliforme
S. ducale
Negreliceras sp. ind.
Nautiloids
N. premolicus/subtenuis
N. subtenuis
Neocomites sp. ind.
"T." pertransiens ?
"T." gratianopolitense ?
S.longi
S.eucyrta
S.uhligi
Sarasinella sp. ind.
T. alpillensis
F. boissieri
B. campylotoxus
B. subcampylotoxus ?
N. neocomiensiformis
L. superba
K. inostranzewi
N. platycostatus
N. teschenensis
N. neocomiensis
Neocomites sp. ind
O. guebhardi
Olcostephanus sp. ind.
Nautiloids
K. pronecostatum
Karakaschiceras sp. ind.
N. peregrinus - found on layer 40 but not in situ
N. peregrinus
Neohoploceras sp. ind.
Himantoceras sp. ind.
Karakachiceras sp. ind. - found on layer 42 but not in situ
B. castellanensis
T. callidiscum ?
T. flucticulum
T. subflucticulum ?
T. subpachydicranum ?
T. pachydicranum
Teschenicera sp. ind.
Criosarasinella ?
O. densicostatus
Neolissoceras sp. ind.
Lytoceras sp. ind.
Bochianites sp. ind.
Nannofossil zonation
Nannofossil events -->
S. colligata
R. dekaenelii
H. peltatus
E. windii
H. circumradiatus
E. striatus
R. wisei
T. verenae
NK zones
NK subzones
CC zones
CC subzones
not studied
CC3
CC4
CC3a
CC3b
CC4a
NK3
NC4
NK3a
NK3b
NC4a

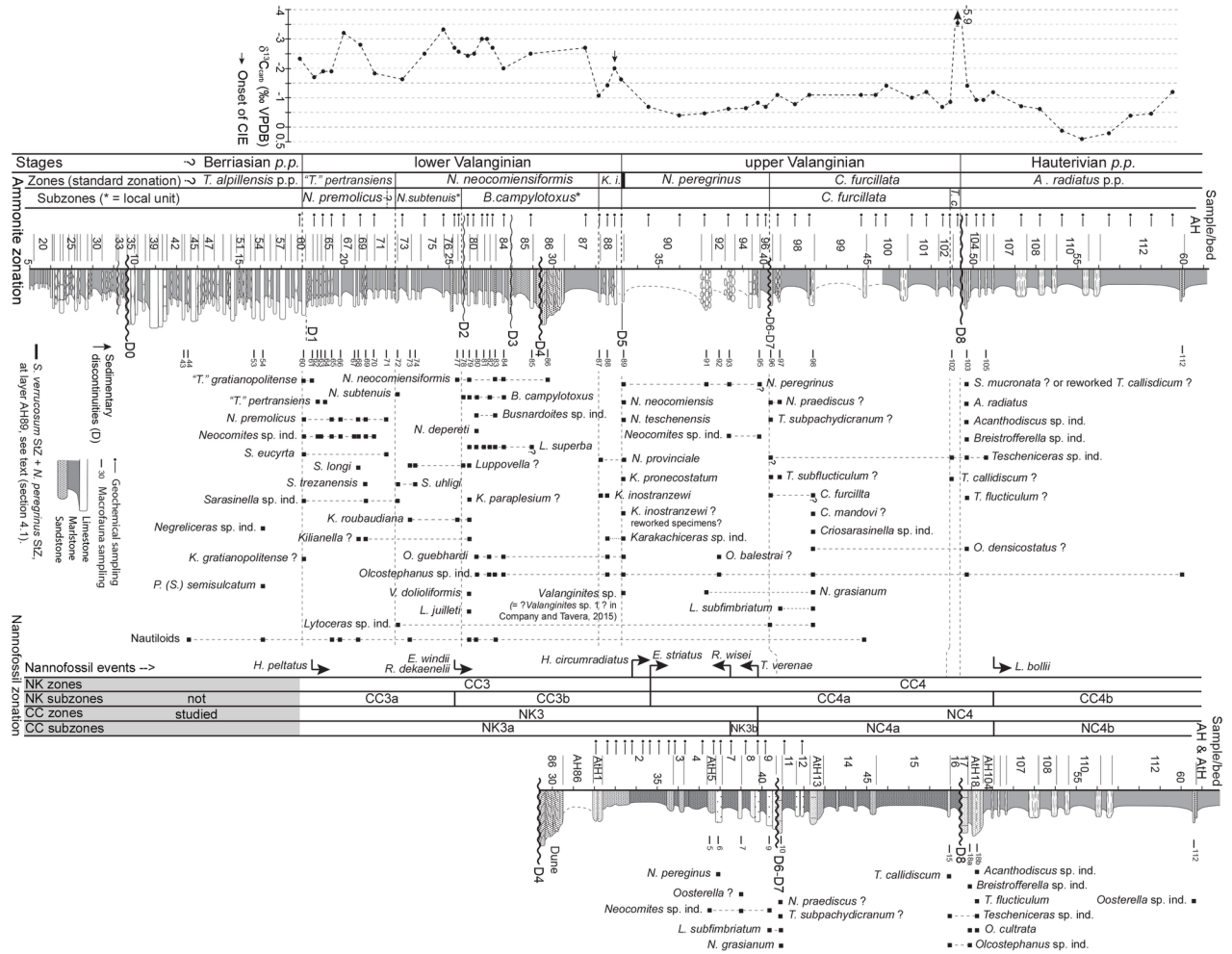
δ13Ccarb (‰ VPDB)
Onset of CIE
Stages
Berriasian p.p.
lower Valanginian
upper Valanginian
Hauterivian p.p.
Zones (standard zonation)
T. alpillensis p.p.
"T." pertransiens
N. neocomiensiformis
K. i.
N. peregrinus
C. furcillata
A . radiatus p.p.
Subzones (* = local unit)
N. premolicus
N.subtenuis*
B.campylotoxus*
C. furcillata
T.c.
Sample/bed
AH
Ammonite zonation
D0
D1
D2
D3
D4
D5
D6-D7
D8
Sedimentary discontinuities (D)
Geochemical sampling
Macrofauna sampling
Limestone
Marlstone
Sandstone
S. verrucosum SIZ + N. peregrinus SIZ, at layer AH89, see text (section 4.1).
"T." gratianopolitense
"T." pertransiens
N. premolicus
Neocomites sp. ind.
S. eucyrta
S. longi
S. trezanensis
Sarasinella sp. ind.
Negreliceras sp. ind.
K. gratianopolitense ?
P. (S.) semisulcatum
N. neocomiensiformis
N. subtenuis
B. campylotoxus
Busnardoites sp. ind.
N. depereti
L. superba
Luppovella ?
S. uhligi
K. paraplesium ?
K. roubaudiana
Kilianella ?
O. guebhardi
Olcostephanus sp. ind.
V. dolioliformis
L. juilleti
Lytoceras sp. ind.
Valanginites sp.
(= ?Valanginites sp. 1 ? in Company and Tavera, 2015)
N. peregrinus
N. neocomiensis
N. teschenensis
Neocomites sp. ind.
N. provinciale
K. pronecostatum
K. inostranzewi
K. inostranzewi ?
reworked specimens?
Karakachiceras sp. ind.
O. balestrai ?
L. subfimbriatum
N. grasianum
N. peregrinus
N. praediscus ?
T. subpachydicranum ?
T. subfluctuculum ?
C. furcillta
C. mandovi ?
Criosarasinella sp. ind.
O. densicostatus ?
S. mucronata ? or reworked T. callisdicum ?
A. radiatus
Acanthodiscus sp. ind.
Breistrofferella sp. ind.
Teschenicera sp. ind.
T. callidiscum ?
T. flucticulum ?
Nautiloids
Nannofossil events -->
H. peltatus
E. windii
R. dekaenelii
H. circumradiatus
E. striatus
R. wisei
T. verenae
L. bollii
Nannofossil zonation
NK zones
NK subzones
CC zones
CC subzones
not studied
CC3
CC4
CC3a
CC3b
CC4a
CC4b
NK3
NK4
NK3a
NK3b
NC4a
NC4b
Sample/bed
AH & AtH
Dune
N. peregrinus
Oosterella ?
Neocomites sp. ind.
L. subfimbriatum
N. grasianum
N. praediscus ?
T. subpachydicranum ?
T. callidiscum
Acanthodiscus sp. ind.
Breistrofferella sp. ind.
T. flucticulum
Oosterella sp. ind.
Teschenicera sp. ind.
O. cultrata
Olcostephanus sp. ind.

Stages
Berriasian p.p.
lower Valanginian
upper Valanginian
Hauterivian p.p.
Zones (standard zonation)
T. alpillensis p.p.
"T." pertransiens
N. neoco.
K. i.
S. verruco.
N. peregrinus
C. furcillata
A. radiatus p.p.
Subzones (* = local unit)
N. premo.
N.s.*
B.c.*
K. prone
C. furcillata
T. c.
Ammonite zonation
Sample/bed
ZS
δ13Ccarb (‰ VPDB)
Onset of CIE
Sedimentary discontinuities (D)
N. premolicus
"T." gratianopolitense ?
Thurmanniceras sp. ind.
Neocomites sp. ind.
S. lohgi
N. neocomiensis
N. platycostatus
N. subtenuis
B. campyloloxus
K. inostranzewi
Karakaschiceras sp. ind.
L. superba ?
Nechploceras sp. ind.
N. provinciale
V. ventrotuberculatus
O. guebhardi
Olcostephanus sp. ind.
N. grasianum
Sarasinella ?
M. rouvillei ?
P. breveti ?
T. alpillensis
T. subfluticulum ?
T. subpachydiranum ?
K. pronecostatum ?
Teschenniceras sp. ind.
Criosarasinella ?
Rodighieroites sp. ind.
R. belimelensis
O. balestrai
Bochianites sp. ind.
Lytoceras sp. ind.
Belemnite
Nautiloids
N. praediscus ?
T. callidiscum ?
T. castellanensiformis ?
A. radiatus
A. Vaceki
B. castellanensis
Breistroffiella sp. ind.
S. mucronata ? or reworked T. callisdicum ?
T. pachydicrarium
T. fluticulum
O. densicostatus ?
L. subfimbriatum
S. verrucosum StSz + K. pronecostatum StSz at ZS52
see text (section 4.1).
Geochemical sampling
Macrofauna sampling
Limestone
Marlstone
Sandstone
Numbering: left column --> right column
38 --> 33
37 --> 32
36 --> 31
35-34 --> 30 (partly?)
D0
D1
D2
D3
D4
D5
D6-7
D8

Stages
Berriasian p.p.
lower Valanginian
upper Valanginian p.p.
Zones (standard zonation)
T. alpillensis p.p.
"T." pertran.
N. premo.
N. neocomiensif.
N. subte.*
B. c.*
K. i.
S. verrucosum
S. ver./K. pro.
N. peregrinus
Subzones (* = local unit)
Ammonite zonation
Sample/bed
IGb-IGz
IGz
IGb
D0
D1
D2
D3
D4-5
base marls 27
Sedimentary discontinuities (D)
F. boissieri
B. calisto
"T." pertransiens ?
N. neocomiensiformis
B. campylotoxus
"T." gratianopolitense ?
Thurmanniceras sp. ind.
Fauriella sp. ind.
Berriasella sp.
L. honnoratianum
H. silesiacum
Negreliceras sp. ind.
N. premolicus
N. premolicus/N. subtenuis
N. subtenuis
Neocomites sp. ind.
Neohoploceras sp. ind.
N. neocomiensis ?
N. platycostatus
K. paraplesium
Karakaschiceras sp. ind.
Sarasinella sp. ind.
N. submartini
K. inostranzewi
Oosterella sp. ind.
Kilianella ?
Neolissoceras sp. ind.
K. roubaudiana
B. neocomiensis
Kilianella sp. ind.
L. superba
O. guebhardi
Olcostephanus sp. ind.
V. ventrotuberculatus
V. doliciformis
Belemnite
Nautiloids
Geochemical sampling
30 Macrofauna sampling
Limestone
Marlstone
Sandstone
$\delta^{13}C_{carb}$ (‰ VPDB)
-5
-4
-3
-2
-1
0

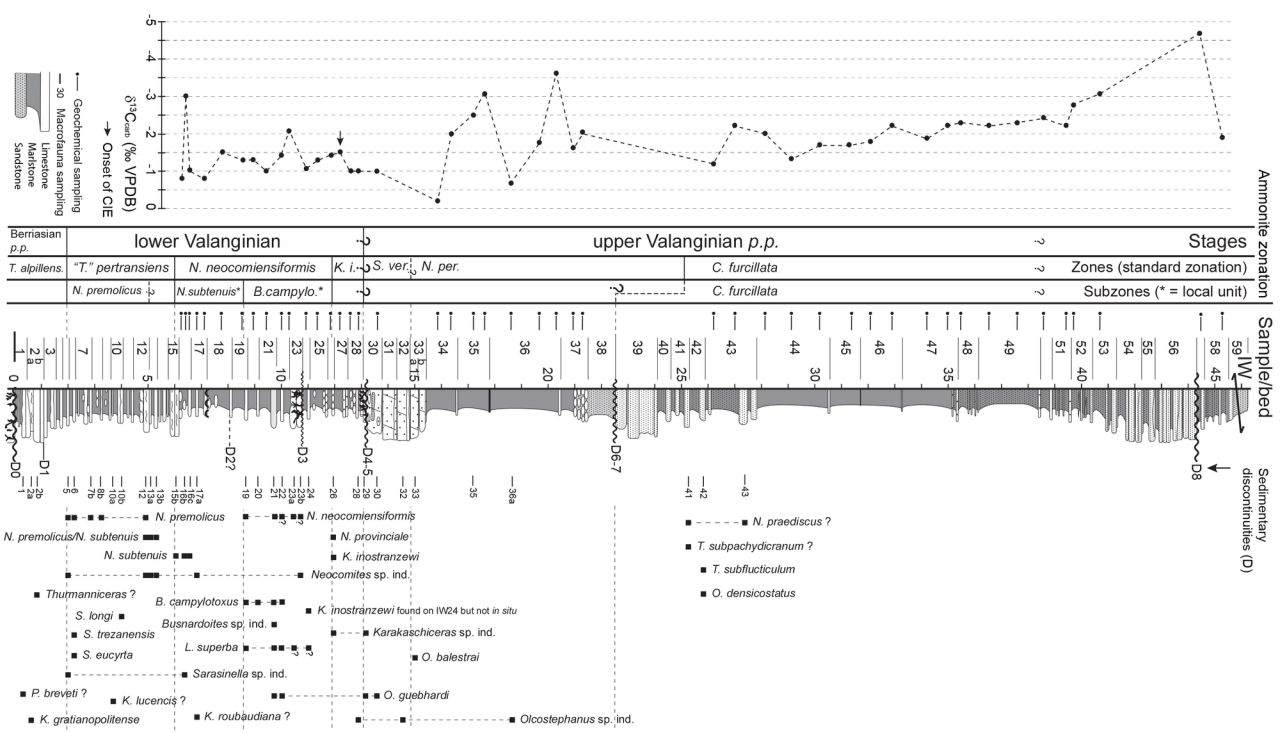
Geochemical sampling
30 Macrofauna sampling
Limestone
Marlstone
Sandstone
δ13Ccarb (‰ VPDB)
Onset of CIE
Ammonite zonation
Berriasian p.p.
lower Valanginian
upper Valanginian p.p.
Stages
T. alpillens.
"T." pertransiens
N. neocomiensiformis
K. i.
S. ver.
N. per.
C. furcillata
Zones (standard zonation)
N. premolicus
N.subtenuis*
B.campylo.*
Subzones (* = local unit)
Sample/bed
IW
D0
D1
D2?
D3
D4-5
D6-7
D8
Sedimentary discontinuities (D)
N. premolicus
N. neocomiensiformis
N. premolicus/N. subtenuis
N. provinciale
N. subtenuis
K. inostranzewi
Neocomites sp. ind.
Thurmanniceras ?
B. campylotoxus
K. inostranzewi found on IW24 but not in situ
S. longi
Busnardoites sp. ind.
Karakaschiceras sp. ind.
S. trezanensis
S. eucyrta
L. superba
O. balestrai
Sarasinella sp. ind.
P. breveti ?
K. lucensis ?
O. guebhardi
K. gratianopolitense
K. roubaudiana ?
Olcostephanus sp. ind.
N. praediscus ?
T. subpachydicranum ?
T. subflucticulum
O. densicostatus

Stages
Berriasian p.p.
low. Val.
upper Valanginian p.p.
Zones (standard zonation)
T. alpillensis p.s.p.
"T." p.
K. i.
N. n.
S. v.
K. pro.
N. peregrinus
C. furcillata p.p.
Subzones (* = local unit)
N. p.
B. c.*
N. s.*
O. nicklesi
Ammonite zonation
Sample/bed
OB
D0
D1
D2+D3?
D4
D5
D6
D7
Sedimentary discontinuities (D)
"T." pertransiens
"T." gratianopolitense
B. campylotoxus
K. inpstranzewi
Groebericeras ?
N. premolicus
N. subtenuis
N. neocomiensiformis
N. teschenensis
N. platycostatus
Neocomites sp. ind.
N. neocomiensis
S. longi
Sarasinella sp. ind.
N. provinciale
V. ventrotuberculatus
S. contestartum
T. alpillensis ?
O. guebhardi
K. pronecostatum
Neohoplites ?
Neohoplites sp. ind. ?
H. acuticostatum
Himantoceras sp. ind.
Oosterella sp. ind.
O. balestrai
Olcostephanus sp. ind.
O. gaudryi (morphe fascigera)
Neolissoceras sp. ind.
C. mandovi ?
Tescheniceras ?
T. subpachydicranum ?
N. praediscus ?
29(pyritized specimens)
28 (pyritized specimens)
S. verrucosum StSz + K. pronecostatum StSz at OB24, see text (section 4.1).
30 Macrofauna sampling
Limestone
Marlstone
Sandstone

South-east France
Vergol-La Charce section, Vocontian Basin
Angles section, Vocontian Basin
Essaouira-Agadir Basin (EAB), this study
Cehegin area, Subbetic Basin
SE Spain
Boissieri
Pertransiens
Campylotoxus
Verrucosum
Trinodosum
Calli.
Radiatus
Loryi p.p.
Ammonite zonation
Nannofossil zonation
Alpillensis p.p.
Otopeta
NC2
CC2
NC3
CC3
NC4
CC4
A
B
L. bollii
E. windii
E. striatus
R. wisei
E. primus
E. windii
R. dekaenelii
C. oblongata
R. wisei
Alpillensis
Pertrans.
Neocom.
Inostr.
Verrucos.
Peregrin.
Furcillata
Radiatus
Loryi
Alpill.
Otopeta
Premolicus
Cam.
Inostr.
Platy.
Verru.
Prone.
Pereg.
Nickl.
Furcill.
Calcid.
Jean.
NK2
NK3
NC4
A
B
Nannofossil events
L. bollii
E. windii
T. verenae
R. wisei
E. windii
C. oblongata
P. fenestrata
Boissieri p.p.
Stephano.
Hirs.
Sub.
Trinodo.
T. verenae
E. striatus
R. wisei
E. windii
C. oblongata
Berriasian p.p.
lower Valanginian
upper Valanginian
Hauterivian p.p.
Stages
Alpill. p.p.
Premolicus
Subtenuis
Ver. ? ~≥ Prone.
Pereg. Nickl.
Furcill.
Calcid.
?
?
T. verenae
R. wisei
E. striatus
E. windii
H. peltatus
S. colligata
C. oblongata
present
L. bollii
T. verenae
R. wisei
H. peltatus
C. oblongata
S. colligata
P. fenestrata
T. verenae
R. wisei
Pctd.
Alpill.
Otopeta
Neoc.
Inostr.
gap
Verrucos.
Peregrin.
Furcillata
Verruc.
Pronec.
Platyc.
Nickl.
not studied

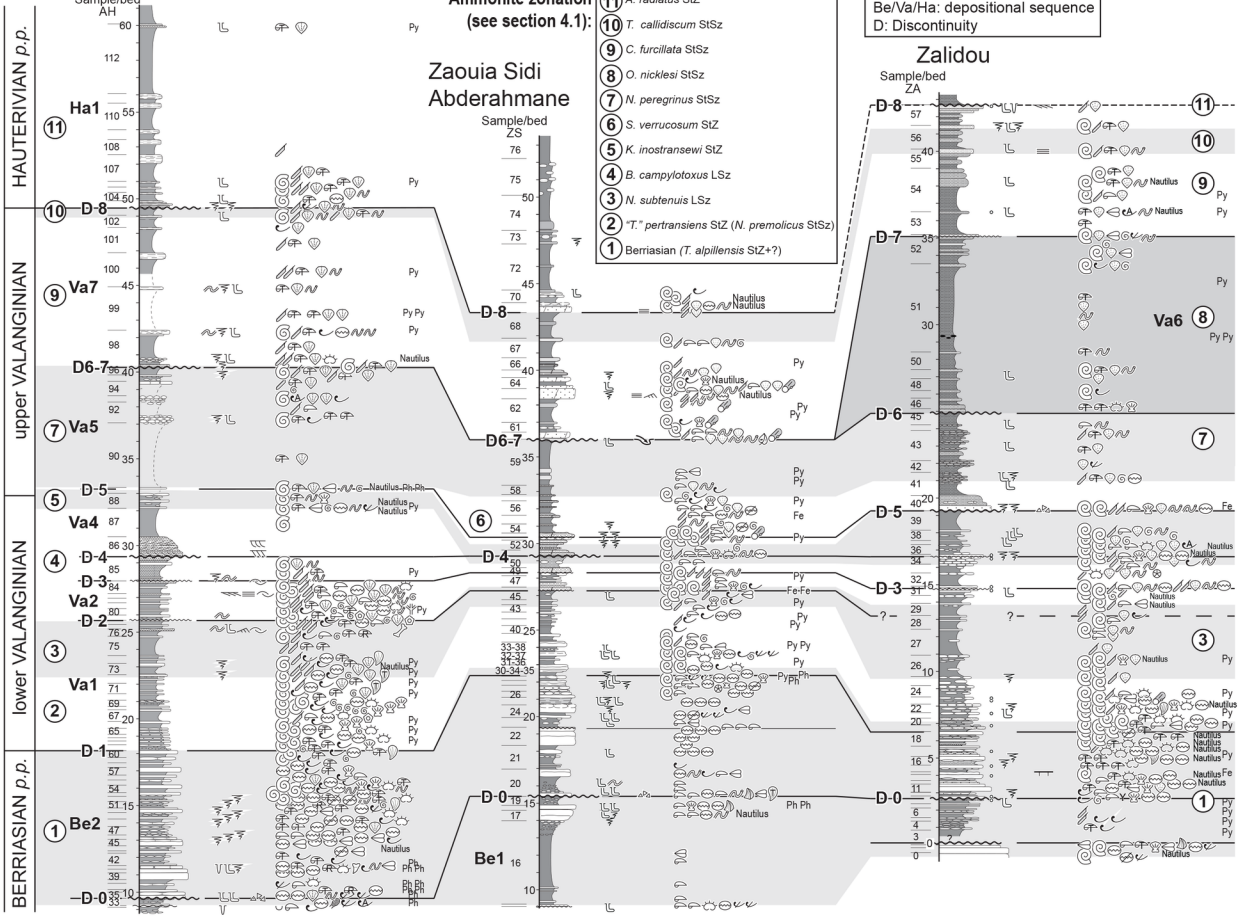
S
Aït Hamouch
13 km
Zaouia Sidi Abderahmane
23 km
N
Zalidou
Sample/bed AH
Sample/bed ZS
Sample/bed ZA
Ammonite zonation (see section 4.1):
11 A. radiatus StZ
10 T. callidiscum StSz
9 C. furcillata StSz
8 O. nicklesi StSz
7 N. peregrinus StSz
6 S. verrucosum StZ
5 K. inostransewi StZ
4 B. campylotoxus LSz
3 N. subtenuis LSz
2 "T." pertransiens StZ (N. premolicus StSz)
1 Berriasian (T. alpillensis StZ+?)
Be/Va/Ha: depositional sequence
D: Discontinuity
HAUTERIVIAN p.p.
upper VALANGINIAN
lower VALANGINIAN
BERRIASIAN p.p.
Ha1
Va7
Va5
Va4
Va2
Va1
Be2
Be1
Va6
D-8
D-7
D-6
D-5
D-4
D-3
D-2
D-1
D-0
Nautilus
Py
Ph
Fe

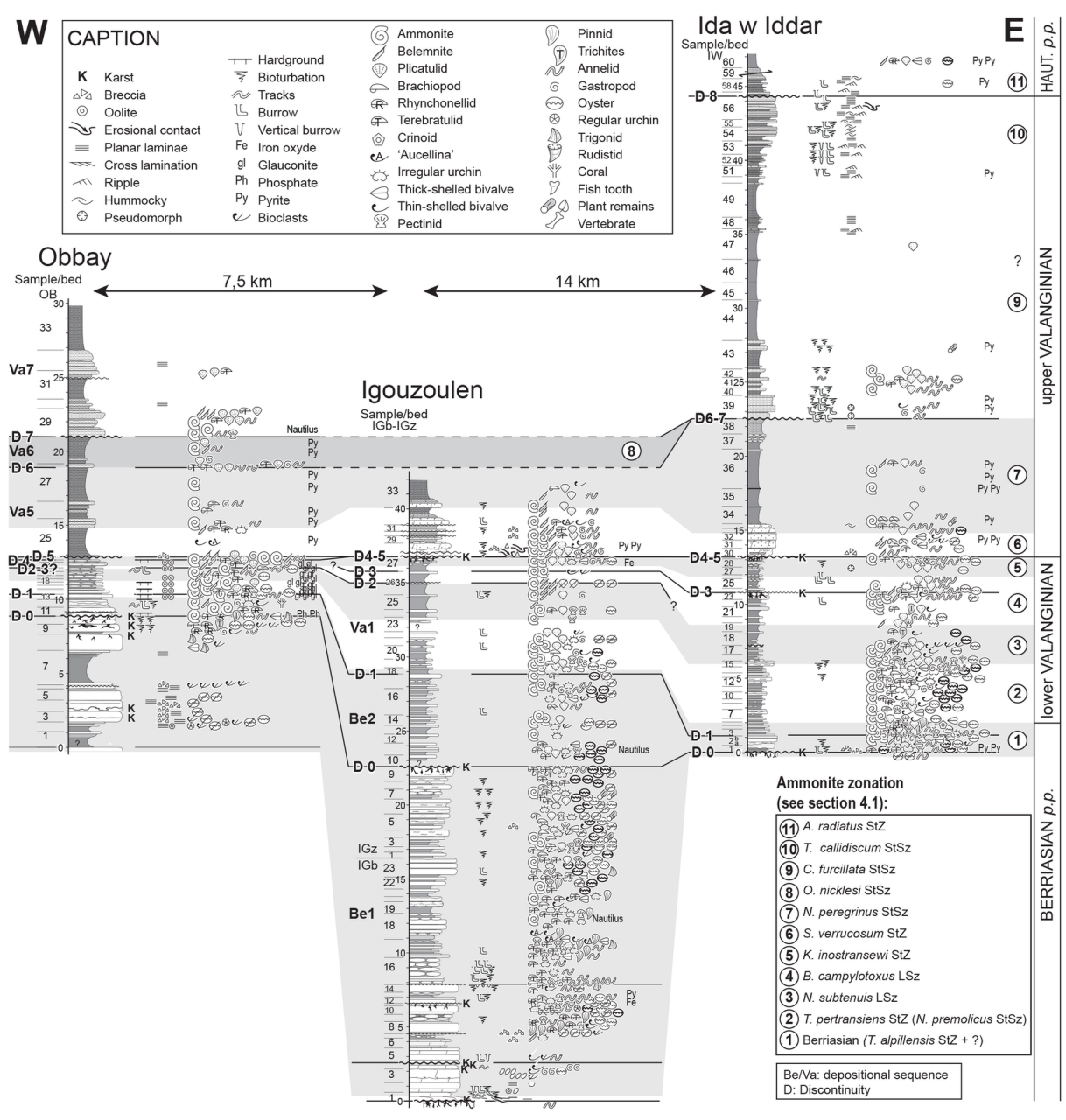
W
E
CAPTION
K Karst
Breccia
Oolite
Erosional contact
Planar laminae
Cross lamination
Ripple
Hummocky
Pseudomorph
Hardground
Bioturbation
Tracks
Burrow
Vertical burrow
Fe Iron oxyde
gl Glauconite
Ph Phosphate
Py Pyrite
Bioclasts
Ammonite
Belemnite
Plicatulid
Brachiopod
Rhynchonellid
Terebratulid
Crinoid
'Aucellina'
Irregular urchin
Thick-shelled bivalve
Thin-shelled bivalve
Pectinid
Pinnid
Trichites
Annelid
Gastropod
Oyster
Regular urchin
Trigonid
Rudistid
Coral
Fish tooth
Plant remains
Vertebrate
Obbay
Sample/bed
OB
7,5 km
14 km
Ida w Iddar
Sample/bed
IW
Igouzoulen
Sample/bed
IGb-IGz
Va7
Va6
Va5
Va1
Be2
Be1
D-7
D-6
D-5
D-4
D2-3?
D-1
D-0
D4-5
D-3
D-2
D6-7
IGz
IGb
Nautilus
Py
Fe
Ph
gl
K
HAUT. p.p.
upper VALANGINIAN
lower VALANGINIAN
BERRIASIAN p.p.
Ammonite zonation
(see section 4.1):
11 A. radiatus StZ
10 T. callidiscum StSz
9 C. furcillata StSz
8 O. nicklesi StSz
7 N. peregrinus StSz
6 S. verrucosum StZ
5 K. inostransewi StZ
4 B. campylotoxus LSz
3 N. subtenuis LSz
2 T. pertransiens StZ (N. premolicus StSz)
1 Berriasian (T. alpillensis StZ + ?)
Be/Va: depositional sequence
D: Discontinuity

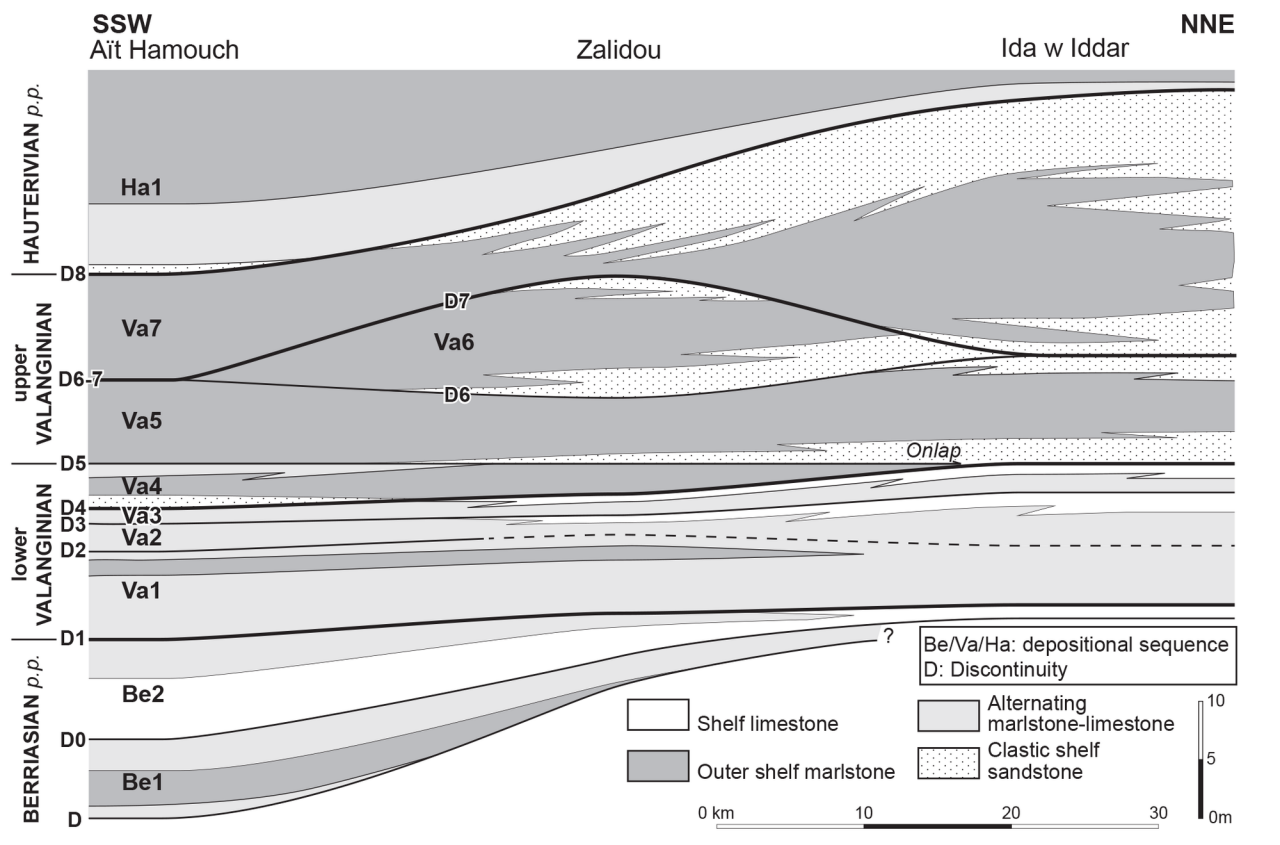
SSW
Aït Hamouch
Zalidou
Ida w Iddar
NNE
HAUTERIVIAN p.p.
upper VALANGINIAN
lower VALANGINIAN
BERRIASIAN p.p.
Ha1
D8
D7
Va7
Va6
D6-7
D6
Va5
D5
Onlap
Va4
D4
Va3
D3
Va2
D2
Va1
D1
?
Be2
D0
Be1
D
Be/Va/Ha: depositional sequence
D: Discontinuity
Shelf limestone
Outer shelf marlstone
Alternating marlstone-limestone
Clastic shelf sandstone
10
5
0m
0 km
10
20
30

Essaouira-Agadir Basin (EAB) - Morocco
Aït Hamouch, simplified section
Zalidou, simplified section
South-east France Basin - Thickness x 1/4
Vergol-La Charce, simplified section, Vocontian Basin
Carajuan simplified, section, Provence Platform
2,5 m
10 m
Zones (standard zonation)
Subzones (* = local unit)
Calcareous nannofossil zonation
Ammonite zonation
T. alpillensis p.p.
T.* pertransiens
N. neocomiensiformis
A. radiatus p.p.
C. furcillata
N. peregrinus
K. v.
B. campylotoxus*
N.subtenuis*
N. premolicus*
not studied
NC4b
NC4a
NK3b
NK3a
D8
D6-D7
D5
D4
D3
D2
D1
D0
Dune
R. wisei
T. verenae
T. c.
S. ver.
K. pro
K. inostran.
N. subtenuis*
B. cam.*
N. premol.
T.* pertr.
N. neocomiensiformis
★ : value = -5.9‰
δ13Ccarb (‰ VPDB)
S. verrucosum StZ + N. peregrinus StZ, see section 4.1.
Limestone or sandstone
Marlstone
Onset of CIE
GSSP
LCH189
upper Valanginian
lower Valanginian
Haut. p.p.
Ber. p.p.
T.* alpi. p.p.
T.* oto.
Unnamed
C. oblongata
Otopeta bundle
SB E
SB D
VGL-B136, base of Valanginian sensu Kenjo et al. (2021)
Stages
Radiatus bundle
Furcillata bundle
Nicklesi bundle
Peregrinus bundle
Pronecostatum bundle
Verrucosum bundle
Barrande
SB H
SB G
SB F
Weissert Event
DVT
DVS
DVM
DCB
Limestone
Marlstone
Formations
F1 p.p.
F2
F3
F4
F5
F6
F7
F8
F9
F10
F11
F12
F13 p.p.
T. alpi.
?/? "T.* pertransiens"
N. neocomiensiformis
K. inostranzewi
V. vernuc.
N. per.
C. f. A. r. p.p.
+1
+2
+3
0
+1
+2
+3
δ13Ccarb (‰ VPDB)